RESEARCH ARTICLE

CLINICAL AND TRANSLATIONAL MEDICINE
Open Access

WILEY

Activation of autophagy reverses progressive and deleterious protein aggregation in PRPF31 patient-induced pluripotent stem cell-derived retinal pigment epithelium cells

Maria Georgiou[1] | Chunbo Yang[1] | Robert Atkinson[1] | Kuan-Ting Pan[2] |
Adriana Buskin[1] | Marina Moya Molina[1] | Joseph Collin[1] | Jumana Al-Aama[3] |
Franziska Goertler[4] | Sebastian E. J. Ludwig[2] | Tracey Davey[1] |
Reinhard Lührmann[2] | Sushma Nagaraja-Grellscheid[4,5] | Colin A. Johnson[6] |
Robin Ali[7] | Lyle Armstrong[1] | Viktor Korolchuk[1] | Henning Urlaub[2,8] |
Sina Mozaffari-Jovin[2,9,10] | Majlinda Lako[1] 🔘

[1]Newcastle University Biosciences
Institute, Newcastle upon Tyne, UK

[2]Max Planck Institute for
Multidisciplinary Sciences, Göttingen,
Germany

[3]Faculty of Medicine, King Abdulaziz
University, Saudi Arabia

[4]Department of Biological Sciences,
University of Bergen, Norway

[5]Department of Biosciences, Durham, UK

[6]Leeds Institute of Molecular Medicine,
University of Leeds, Leeds, UK

[7]King's College, London, UK

[8]Bioanalytics, Department of Clinical
Chemistry, University Medical Center,
Goettingen, Germany

[9]Medical Genetics Research Center,
Mashhad University of Medical Sciences,
Mashhad, Iran

[10]Department of Medical Genetics,
Faculty of Medicine, Mashhad University
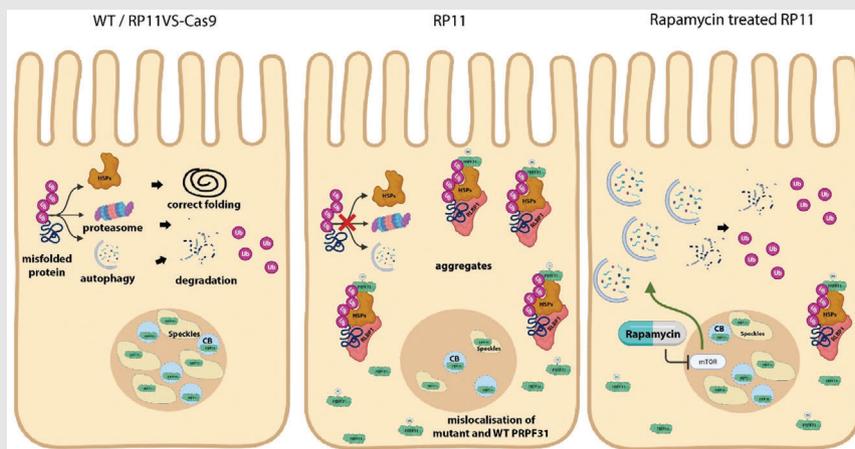of Medical Sciences, Mashhad, Iran

Correspondence
Majlinda Lako, Newcastle University
Biosciences Institute, Newcastle upon
Tyne, UK.
Email: majlinda.lako@ncl.ac.uk
Sina Mozaffari-Jovin, Mashhad University
of Medical Sciences, Mashhad, Iran.
Email: smozaffmp@gmail.com

Graphical Abstract

Schematic presentation shows the localisation of mutant PRPF31 in the cytoplasm of RP11-RPE cells and accumulation of aggregates containing HSPs, visual cycle and ubiquitin conjugated proteins, which were much reduced upon application of autophagy activator, Rapamycin. m-mutant PRPF31, CB-Cajal bodies, Ub-ubiquitin, HSPs-heat shock proteins.

RESEARCH ARTICLE

Activation of autophagy reverses progressive and deleterious protein aggregation in PRPF31 patient-induced pluripotent stem cell-derived retinal pigment epithelium cells

Maria Georgiou[1] | Chunbo Yang[1] | Robert Atkinson[1] | Kuan-Ting Pan[2] |
Adriana Buskin[1] | Marina Moya Molina[1] | Joseph Collin[1] | Jumana Al-Aama[3] |
Franziska Goertler[4] | Sebastian E. J. Ludwig[2] | Tracey Davey[1] |
Reinhard Lührmann[2] | Sushma Nagaraja-Grellscheid[4,5] | Colin A. Johnson[6] |
Robin Ali[7] | Lyle Armstrong[1] | Viktor Korolchuk[1] | Henning Urlaub[2,8] |
Sina Mozaffari-Jovin[2,9,10] | Majlinda Lako[1] 🔘

[1]Newcastle University Biosciences Institute, Newcastle upon Tyne, UK

[2]Max Planck Institute for Multidisciplinary Sciences, Göttingen, Germany

[3]Faculty of Medicine, King Abdulaziz University, Saudi Arabia

[4]Department of Biological Sciences, University of Bergen, Norway

[5]Department of Biosciences, Durham, UK

[6]Leeds Institute of Molecular Medicine, University of Leeds, Leeds, UK

[7]King's College, London, UK

[8]Bioanalytics, Department of Clinical Chemistry, University Medical Center, Goettingen, Germany

[9]Medical Genetics Research Center, Mashhad University of Medical Sciences, Mashhad, Iran

[10]Department of Medical Genetics, Faculty of Medicine, Mashhad University of Medical Sciences, Mashhad, Iran

Correspondence
Majlinda Lako, Newcastle University Biosciences Institute, Newcastle upon Tyne, UK.
Email: majlinda.lako@ncl.ac.uk
Sina Mozaffari-Jovin, Mashhad University of Medical Sciences, Mashhad, Iran.
Email: smozaffmp@gmail.com

Abstract

Introduction: Mutations in pre-mRNA processing factor 31 (*PRPF31*), a core protein of the spliceosomal tri-snRNP complex, cause autosomal-dominant retinitis pigmentosa (adRP). It has remained an enigma why mutations in ubiquitously expressed tri-snRNP proteins result in retina-specific disorders, and so far, the underlying mechanism of splicing factors-related RP is poorly understood.

Methods: We used the induced pluripotent stem cell (iPSC) technology to generate retinal organoids and RPE models from four patients with severe and very severe PRPF31-adRP, unaffected individuals and a CRISPR/Cas9 isogenic control.

Results: To fully assess the impacts of *PRPF31* mutations, quantitative proteomics analyses of retinal organoids and RPE cells were carried out showing

RNA splicing, autophagy and lysosome, unfolded protein response (UPR) and visual cycle-related pathways to be significantly affected. Strikingly, the patient-derived RPE and retinal cells were characterised by the presence of large amounts of cytoplasmic aggregates containing the mutant PRPF31 and misfolded, ubiquitin-conjugated proteins including key visual cycle and other RP-linked tri-snRNP proteins, which accumulated progressively with time. The mutant PRPF31 variant was not incorporated into splicing complexes, but reduction of PRPF31 wild-type levels led to tri-snRNP assembly defects in Cajal bodies of PRPF31 patient retinal cells, altered morphology of nuclear speckles and reduced formation of active spliceosomes giving rise to global splicing dysregulation. Moreover, the impaired waste disposal mechanisms further exacerbated aggregate formation, and targeting these by activating the autophagy pathway using Rapamycin reduced cytoplasmic aggregates, leading to improved cell survival.

Conclusions: Our data demonstrate that it is the progressive aggregate accumulation that overburdens the waste disposal machinery rather than direct PRPF31-initiated mis-splicing, and thus relieving the RPE cells from insoluble cytoplasmic aggregates presents a novel therapeutic strategy that can be combined with gene therapy studies to fully restore RPE and retinal cell function in PRPF31-adRP patients.

KEYWORDS
aggregate formation, autophagy, human pluripotent stem cells, proteasome, PRPF31, retinal organoids, retinitis pigmentosa, RPE, tri-snRNP assembly defects, UPR

1 | INTRODUCTION

Misfolding, aggregation and deposition of abnormal proteins are a common hallmark event of multiple neurodegenerative diseases (NDs). Aberrant accumulation of self-aggregating proteins intracellularly and extracellularly causes cellular toxicity due to the formation of insoluble non-native aggregates, which disrupt protein homeostasis and eventually lead to cellular dysfunction or cell death.[1] Although protein aggregates differ in protein composition, size and structure in distinct NDs, they share common cytotoxic effects and accumulate progressively over time.[2]

Aggregation and accumulation of misfolded proteins over time are also common features of many retinal dystrophies including age-related macular degeneration and retinitis pigmentosa (RP).[3] RP is the most common among all inherited retinal disorders causing blindness, with an incidence of 1 in 4000 people, and more than 1 million affected individuals worldwide.[4] The progressive degeneration of photoreceptor cells and retinal pigmented epithelium (RPE) cells are the major pathological events in autosomal dominant RP,[5] which constitute approximately 43% of all known RP cases.

Up to date, more than 80 genes have been implicated in non-syndromic RP. These include genes that encode retinal-specific proteins such as *Rhodopsin* (*RHO*), the most frequently affected gene in RP, associated with the formation of cellular aggregates.[6] Particularly, *RHO* [P23H], which is the most common mutation in RP, produces an extremely aggregation-prone form of rhodopsin failing to translocate to the plasma membrane to form the visual pigment.[3] These aggregates are ubiquitinated and targeted for degradation by the proteasome,[6] however, saturation of the proteolytic machinery enhances the accumulation of rhodopsin aggregates.[7]

In addition to the genes encoding retinal-specific proteins, mutations in genes encoding pre-mRNA processing factors (*PRPFs*) have been associated with retina-specific diseases, despite their ubiquitous expression.[8] PRPFs, including PRPF3, PRPF4, PRPF6, PRPF8, PRPF31, and SNRNP200, are all components of the U4/U6.U5 tri-snRNP complex, which is a major constituent of the spliceosome— a large macromolecular complex essential for the catalysis of pre-mRNA splicing.[9] Mutations in *PRPFs* constitute ~15% of autosomal-dominant retinitis pigmentosa (adRP) cases and affect the assembly of

the spliceosome leading to mis-splicing of genes important for retinal function.[10] Published evidence indicates that mammalian cells with *PRPF* mutations are characterised by accumulation of less soluble proteins that are prone to aggregation.[11] For example, mutations in *PRPF3* affect the localisation of PRPF3 protein itself leading to the aggregation of misfolded proteins, which triggers the apoptosis of photoreceptor cells.[11] However, the role of misfolded aggregates in disease pathogenesis and their association with photoreceptor cell death and/or RPE has not been fully understood.

About 10% of adRP cases are caused by mutations in *PRPF31*, which is an important component of the splicing machinery required for the assembly and stability of tri-snRNPs.[12] This type of RP is known as RP11. Using iPSC-based modelling and differentiation to retinal cells, we previously reported the presence of large deposits on the basal side of RP11-RPE cells. Importantly, patient-specific RPE (but not photoreceptor cells or non-retinal cells) were characterised by the presence of mutant PRPF31 protein, suggesting that RPE cells are the most affected cell type.[10] Recently, findings by Diaz-Corrales and colleagues in the Prpf31$^{\text{p.A216P/+}}$ mouse model have demonstrated the aggregation of mutant *PRPF31* protein in the cytoplasm of RPE cells, accompanied by the overexpression of HSPA4L chaperone.[13]

Molecular chaperones act as the initial defence cellular mechanism in response to misfolded proteins damaged by mutations or stress. Under normal conditions, chaperones protect cells by stabilisation of folding intermediates and prevention of protein misfolding and aggregation. However, misfolded proteins that are unable to reassemble correctly are ubiquitinated and targeted for degradation by the proteolytic degradation machinery. In the case where unfolded protein response (UPR) malfunctions, an intrinsic apoptotic pathway is activated as a secondary response to degrade accumulated proteins. However, dysregulation of autophagy often leads to protein aggregation diseases.[14]

In this study, we have used induced pluripotent stem cell-derived RPE (iPSC-RPE) from patients harbouring two different *PRPF31* mutations to investigate their impact on the proteome and phenome of RPE cells. We show that the mutant PRPF31 protein is mis-localised, accumulated and aggregated in the cytoplasm of RP11-RPE cells in association with misfolded, ubiquitin-conjugated proteins. Importantly, we provide evidence that protein degradation and waste disposal mechanisms are impaired in RP11-RPE cells, leading to the accumulation and deposition of large aggregates, which affect RPE cell survival. Activation of autophagy by Rapamycin enhanced the clearance of cytoplasmic aggregates and improved cell survival.

2 | MATERIALS AND METHODS

2.1 | Human cell lines

All samples used in this study were obtained with informed consent according to the protocols approved by Yorkshire and the Humber Research Ethics Committee (REC ref. no. 03/362). PRPF31-iPSC lines used in this study were derived from four patients with severe (RP11S1, RP11S3), moderate (RP11M) and very severe (RP11VS) phenotypes as described in our earlier work.[10] RP11VS, RP11M and RP11S1 cell lines harbour the same *PRPF31* mutation (c.1115_1125 del11) but vary in the severity of the disease. RP11S3 patients harbour a different mutation (c.522_527+10del). Crispr/Cas9 isogenic (Cas9-RP11VS) and unaffected cell lines (WT1, WT2 and WT3) were used as controls.[10] Throughout the paper, we will refer to Crispr/Cas9 as isogenic control and unaffected as control.

2.2 | iPSC culture

Human iPSCs were cultured on pre-coated with growth factor reduced Matrigel (Corning, 354230) six-well plates. mTeSR™1 (StemCell Technologies, 05850) media supplemented with penicillin/streptomycin (Gibco, 15140) was used on daily basis for the culturing of iPSCs. Passaging of iPSCs was carried out every 4–5 days using Versene (ethylenediaminetetraacetic acid [EDTA] 0.02%) (Lonza, BE17–771E) solution for 3–5 min at 37°C. The cells were transferred to fresh pre-coated six-well plates in a ratio 1:6. The cells were maintained at 37°C, in a humidified environment, with 5% CO_2. Cryopreservation of iPSCs was performed using freezing media containing 90% foetal bovine serum (Gibco, 10270) and 10% dimethyl sulfoxide (Sigma, D2650) and 10 μM Rock inhibitor (Y-27632, Chemdea, CD0141).

2.3 | Differentiation of iPSCs to RPE cells

Control and patient-derived iPSCs were grown on Matrigel coated six-well plates using mTeSR™1 media. To differentiate iPSCs to RPE cells, a directed differentiation protocol was performed as described in a recent publication.[15] Specifically, when 80%–95% confluency was reached, mTeSR™1 media was replaced with 2 ml of differentiation medium (DMEM; High Glucose, 50 μM β-mercaptoethanol, 1 × minimal essential medium (MEM) non essential amino acids (NEAA), 20% knockout serum (KOS) and 10 mM Nicotinamide) from day 0 to day 7. Subsequently, from day 7 to day 14, nicotinamide was replaced

with 100 ng/ml Activin A. Thereafter, nicotinamide was substituted with 3 μM CHIR99021 (Sigma, SML1046) from day 14 to 42. From day 42 onwards until harvesting of the RPE patches, the cells were fed three times a week with differentiation medium containing DMEM (High Glucose), 50 μM β-mercaptoethanol, 1 × MEM NEAA and 4% KOS. RPE patches were mechanically collected around day 90 using a blade. The collected RPE patches were dissociated in TrypLE (10 ×) (Invitrogen, USA) for 20 min at 37°C. The RPE cells were sieved using a 100 μm cell strainer and re-plated at 1.5 × 10^5 cells per cm^2 on 12-well plates or on 24 Transwell inserts (GreinerBioOne, 662641).

2.4 | Differentiation of iPSCs to retinal organoids

iPSCs were dissociated to single cells using Accutase (Gibco, A1110501) and 7,000 cells were seeded into each well of Lipidure-coated 96-well U-bottomed plate (Amsbio AMS LCP-A-U96-6) and cultured in mTeSR-1 medium supplemented with 10 μM ROCK inhibitor Y-27632 (Chemdea, CD0141) to form Embryonic Bodies. After 48 h, the media was changed to differentiation medium containing 45% Iscove's modified Dulbecco's medium (Gibco, 12440–053), 45% Hams F12 (Gibco, 31765–029), 10% KSR (Gibco, 10828–028), 1× GlutaMAX (Gibco, 35050–038), 1% chemically defined lipid concentrate (Thermo, 11905031), 450 μM monothioglycerol (Sigma, M6145) and 1× penicillin/streptomycin (Gibco, 15140–122). This was defined as day 0 of differentiation. From day 6 to day 9, 1.5 nM BMP4 (R&D, 314-BP) was added to the differentiation medium. From day 18, the culture medium was changed to 10% fetal bovine serum (Gibco, 10270–106) in DMEM/F12 (Gibco, 31330–038) supplemented with 1× N2 (Thermo, A1370701), 0.1 mM Taurine (Sigma, T8691) and 0.5 uM Retinoic Acid (Sigma, R2625), 0.25 μg/ml Fungizone (Gibco, 15290–02) and penicillin/streptomycin (Gibco, 15140–122) until day 150.

2.5 | Western blotting

Cell culture samples were washed three times with phosphate buffered saline (PBS) and collected. RPE cells were collected using a cell scraper and retinal organoids were manually transferred into 15 ml Falcon tubes and precipitated by gravity. Cell culture samples were re-suspended in lysis buffer (25 mM Tris-Cl pH 7.5, 120 mM NaCl, 1 mM EDTA pH 8.0, 0.5% Triton X100) supplemented with protease inhibitors (Roche 11697498001) and vortexed for 15 min at 4°C followed by ultra-sonication three times 5 sec each (Bradson Sonifier150) to obtain the whole cell lysate. The protein concentration was determined using the Bradford Dye Reagent (Bio-Rad 500-0205). Ten micrograms of whole cell lysate was applied to sodium dodecyl sulfate-polyacrylamide gel electrophoresis (SDS-PAGE) and transferred to Hybond polyvinylidene difluoride (PVDF) membrane (GE Health 15259894). PVDF membranes were blocked for 1 h in 5% dried skimmed milk in tris-buffered saline and Tween™ 20 solution (TBST). Thereafter, the membranes were incubated overnight at 4°C with primary antibodies in blocking buffer (Table S1). Washing of the membranes was performed using TBST and the bound primary antibodies were detected using horseradish peroxidase (HRP)-conjugated secondary antibodies (Table S1). Signal was detected by using SuperSignal West Pico PLUS Chemiluminescent Substrate (ThermoFisher) and visualised by Amersham Imager 600 (GE Healthcare Bio-Sciences AB) imager. The signal intensity was quantified by Image Studio Lite v5.2 (LI-COR Biosciences).

2.6 | Immunofluorescence analysis in RPE cells

iPSC-derived RPE cells grown on 24-well PET hanging cell culture inserts (Merck) (pore size 0.4 μm) were fixed with 4% paraformaldehyde (PFA) (Sigma, 47608) for 20 min at room temperature. Before blocking, the pigmentation of RPE cells was removed using Melanin Bleach Kit (Polysciences), followed by 3 washes with PBS. RPE cells were blocked in PBS supplemented with 10% donkey serum and 0.3% Triton-X100 (Sigma, T8787) to permeabilised the cells, for 1 h at room temperature. For p62 and LC3, methanol fixation was used instead and no bleaching prior to immunostaining was carried out. The RPE cells were incubated with primary antibodies overnight at 4°C (Table S1). Following three washes with PBS, RPE cells were incubated with secondary antibodies (Table S1) diluted in solution (PBS, 1% donkey serum, and 0.1% Triton X-100) and stored overnight at 4°C. Nuclei were stained with Hoechst (Life Technologies, UK). Then, RPE cells were mounted with Vectashield and sealed with a coverslip. RPE cells were imaged using the Axio Imager upright microscope with Apotome structured illumination fluorescence using 20× objective, 40× and 63× oil objectives (Zeiss, Germany). Images were presented as a maximum intensity projection and adjusted for brightness and contrast in Adobe Photoshop (Adobe Systems).

2.7 | Immunofluorescence analysis of retinal organoids

Retinal organoid sections were separated using ImmEdge pen (VectorLabs, H-4000) and air-dried for 20 min at room

temperature, followed by three washes with PBS for 5 min to remove OCT 91 from the tissue. Sections were incubated with a blocking solution (5% goat/donkey serum, 0.3% Triton-X in PBS) for 1 h at room temperature. Then, the organoids were incubated overnight at 4°C with primary polyclonal non-conjugated antibodies (Table S1) diluted in antibody diluent (1% bovine serum albumin (BSA, Sigma, A9418), 0.3% Triton-X in PBS). Therefore, the sections were washed thrice with PBS for 15 min each, and secondary conjugated to fluorophores antibodies (Table S1) were diluted in antibody diluent and added to the sections for 1 h at room temperature. To remove unspecific binding, sections were washed three times with PBS for 10 min each. Sections of retinal organoids were covered by Hoechst nuclear stain (Sigma, B2261) diluted in Vectashield at 1:2000 (VectorLabs, H-1000), followed by sealing of the slides by a coverslip.

2.8 | Fluorescence in situ hybridisation

Fluorescence in situ hybridisation (FISH) was performed using probes labelled with Alexa 647 at the 5′-end. The sequences of probes and the RNA-FISH method were as previously described.[16,17] After FISH, cells were immunostained for coilin and prepared for confocal microscopy as described above. Quantification of mean intensities was performed with the ImageJ/Fiji software from four independent measurements.

2.9 | Transmission electron microscopy

Trans-wells of RPE cells were washed with PBS and then fixed with 2% gluteraldehyde in 0.1 M sodium cacodylate buffer. The samples were further fixed in 1% osmium tetroxide, dehydrated in gradient acetone and embedded in epoxy resin. Sections of 70 nm thickness were picked up on copper grids, stained with uranyl acetate and lead citrate and imaged using a Philips CM100 transmission electron microscope with high-resolution digital image capture.

2.10 | Proteasome activity assay

RPE cells from control and patient cell lines were washed with PBS and collected using a cell scraper. Pellets were resuspended in lysis buffer containing 0.5% NP-40 supplemented in distilled water and incubated on ice for 30 min followed by centrifugation at 13,000 ×g for 20 min at 4°C. The supernatant was collected and analysed by Pierce BCA Protein Assay kit (Pierce, ThermoFisher Scientific) to measure the protein concentration. Proteasome sub-

strate Bz-VGR-AMC (BW9375, Biomol International) was used to measure the trypsin like activity of the proteasome. As a control, proteasome inhibitor, MG132, was used. The trypsin-like activity was measured at excitation/emission wavelength of 360 nm/460 nm, respectively, using a Varioskan LUX multimode Microplate reader (ThermoFisher Scientific).

2.11 | Isolation of insoluble fractions in RPE cells

RPE cells were washed with PBS and collected using a cell scraper. Cell pellets were lysed using lysis buffer containing 10 mM Tris-HCL (Sigma, 1185-53-1), pH 7.5, 5 mM EDTA, 1% NP-40 (Sigma, 127087-87-0), 0.5% deoxycholate, 150 mM NaCl (Sigma, 7647-14-5) and 1 complete ULTRA tablet (EDTA, free protease inhibitor; Sigma, 06 538 282 001). The lysates were incubated on ice for 15 min followed by vortexing at 4°C for 15 min. Thereafter, the lysates were sonicated and centrifuged for 15 min at 13,000 ×g. The generated supernatant was transferred in a fresh tube and labelled as the soluble fraction. The remaining pellets were mixed with 20 μl of a lysis buffer (60 mM Tris-HCL, Sigma, 10812846001) pH 7, 2% SDS and, 2.5% 2-Mercaptoethanol (Sigma, 60-24-2), and sonicated. Thereafter, the samples were centrifuged at 16,000 ×g for 20 min at 4°C and the collected supernatant was labelled as the insoluble fraction.

2.12 | Quantification of aggregates

Quantification of cytoplasmic volume was performed using Huygens Image Analysis Software. In brief, two measurements were made per image: one of the total signal and the other of the nuclear signal. Total volume was measured by selecting all the objects from a specific channel in the image and adding the individual volumes together. To calculate cytoplasmic volume, the nuclear volume was subtracted from the total volume. Nuclear objects were defined as objects that colocalised with Hoechst.

2.13 | Statistical analysis

Statistical analysis was perfumed using Prism (GraphPad, USA). Comparisons between variables and statistical significance between groups were performed using analysis of variance (ANOVA) or two-tailed Student's t-test. Error bars represent standard error of the mean (SEM) unless indicated otherwise. Statistical significance was established as indicated by asterisks *$p < 0.05$, **$p < 0.01$, ***$p < 0.001$ and ****$p < 0.0001$.

2.14 | Drug treatments

RPE cells were treated with Rapamycin (500 nM), Trehalose (50 mM), Arimoclomol (1 μM), Salubrinal (25 μM) and STF-083010 (50 μM) of which final concentrations were prepared using dimethylsulfoxide (DMSO) for all drugs, apart from Trehalose which was prepared using distilled water. RPE cells were treated for 7 days with daily media changes containing freshly added drugs. The concentrations were selected based on previous studies.[18–22]

3 | AUTOPHAGY FLUX

RP11VS and Cas9-RP11VS RPE cells were treated in the presence or absence of Bafilomycin (400 nM) (Sigma, B1793) for 4 h to block autophagosome–lysosome fusion. DMSO was used as a vehicle control. Following 4 h of incubation with or without Bafilomycin, RP11VS and Cas9-RP11VS RPE cells were washed with PBS, collected and prepared for Western Blot analysis as described above.

3.1 | Treatment of RPE cells with photoreceptor outer segments

RPE cells were treated with photoreceptor outer segments (POSs) or POS-FITC (20 POSs/cell), after cooling of RPE cells for 30 min at 17°C. After incubation of RPE cells with POSs or POS-FITC, media was removed and replaced with POS suspension immediately, following by incubation at 17°C for another 30 min. This was performed to maximise binding of POSs in RPE cells. Following incubation for 30 min, media was aspirated and replaced with fresh warmed media to remove unbound POS. RPE cells kept in a humidified incubator at 37°C with 5% CO_2. RPE cells were collected at 0, 48, 96, 144 h post-POS feeding. The RPE cells were washed with PBS twice and then fixed with 4% PFA before immunohistostaining.

3.2 | Analysis of snRNP levels by glycerol gradient fractionation and Northern blotting

Retinal organoids or RPE cells were washed with PBS, harvested by centrifugation and pellets were resuspended in 20 mM HEPES-KOH, pH 7.9, 100 mM KCl, 10% (v/v) glycerol, 0.2 mM EDTA, 1 mM DTT and RNasin (1.5 U/μl: Promega). Whole-cell extracts were prepared by sonication (three times bursts at 30% for 5 s on ice, and 30 s pauses in between bursts. Sonicated lysates were centrifuged at 15,000× g for 20 min at 4°C, and were aliquoted, flash frozen and stored at −80°C. Whole-cell extracts (350 μg

each) were diluted with an equal volume of gradient buffer (G150: 20 mM HEPES pH 7.9, 150 Mm NaCl, 1.5 mM $MgCl_2$ and 0.5 mM DTT) and sedimented on linear 4 ml 10%–30% (v/v) glycerol gradients in the G150 buffer. After ultracentrifugation in a Sorvall TH-660 rotor for 14 h at 29,000 rpm, the gradients were fractionated into 24 fractions. To analyse the relative levels of snRNPs, proteins in each gradient fraction were digested with Proteinase K in 20 mM HEPES-KOH pH 7.9, 150 mM NaCl, 10 mM EDTA and 1% (w/v) SDS for 45 min at 42°C. The total RNAs were extracted with phenol/chloroform/isoamylalcohol and were precipitated with ethanol. The isolated RNAs were separated by denaturing 8% urea PAGE followed by Northern blotting and hybridisation with 5′-end radiolabeled probes against U1, U2, U4, U6 and U5 snRNAs,[16] and autoradiography by a Typhoon Trio+ imager (GE Healthcare). To analyse the distribution of selected splicing proteins across the gradients, proteins were precipitated from even-numbered gradient fractions and separated on NuPAGE 4%−12% Bis–Tris gels (Invitrogen) followed by blotting on Hybond enhanced chemiluminescence (ECL) nitrocellulose membranes (GE Healthcare). Immunostaining for PRPF8, Snu114 and PRPF31 was performed using specific antibodies and the Amersham ECL detection kit (GE Healthcare).

3.3 | TMT labelling for mass spectrometry

Total cell lysates were prepared from RP11 and control retinal organoid or RPE cells using Pierce Mass Spec Sample Prep Kit (Thermo Scientific). Lysates were diluted to 120 μl and sonicated. Protein concentrations were determined using the Pierce BCA protein assay kit (Thermo Scientific) and 100 μg of the total proteins from each cell line were labelled with 6-plex isobaric tandem mass tag (TMT6) reagents (Thermo Scientific) following the manufacturer's instruction. To this end, samples were reduced by the addition of tris(2-carboxyethyl)phosphine, alkylated with iodoacetamide and acetone precipitated. Protein pellets were resuspended in 50 mM triethyl ammonium bicarbonate (TEAB) buffer and were digested with trypsin overnight at 37°C. For retinal organoid samples, the patient RP11S1, RP11M, RP11S2 lines and control WT2, WT3 samples were, respectively, labelled with TMT6-128, TMT6-129, TMT6-130 and TMT6-126, TMT6-127 reagents for 1 h at room temperature. For RPE samples, the patient RP11S1, RP11VS, RP11S3 lines and control WT1 samples were, respectively, labelled with TMT6-127, TMT6-128, TMT6-129 and TMT6-126 reagents. Proteomics data from RP11VS and isogenic control RPE cells and retinal organoids obtained in our early study were also included for analysis.[10] Reactions were quenched by 5% hydroxylamine for 15 min.

Fifty micrograms of TMT-labelled peptides from RP11 and control cells were combined and cleaned up using C18 spin columns (Harvard Apparatus), dried by SpeedVac (Eppendorf) and subjected to peptide pre-fractionation using high-pH reversed-phase chromatography. After constituting the dried, TMT-labelled peptides in 100 μl buffer A (10 mM NH_4OH), 50 μl of peptide mixtures were injected into an XBridge BEH C18 HPLC column (150 mm × 1 mm ID, 3.5 μm; Waters) and separated in 80 fractions using a gradient of buffer B (10 mM NH_4OH, 80% acetonitrile) over 90 min. Collected fractions were combined into 20 fractions, dried and resuspended in 20 μl of 0.1% trifluoroacetic acid (TFA) for mass spectrometry analysis.

3.4 | LC−MS/MS analysis

Peptides in each fraction were analysed in three replicates using either an Orbitrap Fusion or a Q Exactive HF-X mass spectrometer (Thermo Fisher Scientific), both coupled with an UltiMate 3000 RSLCnano HPLC system (Thermo Fisher Scientific), as previously described.[10]

3.5 | Data processing

MS/MS spectra were searched against a Swiss-Prot human database containing 20,341 reviewed protein entries using Mascot algorithm (Matrix Science) via Proteome Discoverer 2.2 (PD, Thermo Fisher Scientific) and were processed as previously described.[10] At least two quantifiable unique peptides in each replicate were required for protein quantification. Protein ratios were log transformed and then median normalised in Perseus. These data were combined with our previous proteomic data from RP11VS and the isogenic control.[10] The reported RP11/control ratios are the average of at least two replicates. To identify the differentially expressed (DE) proteins, those proteins with mean a log2 fold change (LFC) less than −0.5 or greater than +0.5 were defined as DE. Gene ontology (GO) enrichment analyses were carried out by Metascape (p-value cut-off 0.02)[23] or by the Perseus software version 1.6.2.2 with a Benjamin–Hochberg false discovery rate 2%.[24]

4 | RESULTS

4.1 | Cytoplasmic mislocalisation of the mutant PRPF31 protein and altered morphology of nuclear speckles in RP11-retinal cells

Given the ubiquitous expression of PRPF31, the specificity of RP mutations to the retinal tissue has remained an enigma for the pathogenesis mechanism of PRPFs-related RP disease. In earlier work, we have compared PRPF31 expression in RPE cells and retinal organoids derived from RP patients in Western blots and shown decreased PRPF31 expression as well as expression of long mutant form of PRPF31 in the RP11-RPE cells.[10] Herein, to assess the localisation of the wild-type and mutant forms of PRPF31 in detail, we first performed immunofluorescence (IF) analysis in three RP11-RPE cells using an antibody against the N-terminus of PRPF31 that detects both the wild-type and mutant proteins. Clear differences were observed with PRPF31 being localised in the nucleus of control RPE cells and predominantly in the cytoplasm of RP11-RPE cells (Figure 1A). Additionally, the tight junctions stained with ZO1 antibody were disrupted in RP11-RPE cells compared to the control cells (Figure 1A), corroborating previously observed tight and adherens junction associated protein modifications in the retina of animal model of adRP.[25]

To distinguish localisation of PRPF31 variants in soluble and insoluble fractions, a Western blot of the two fractions was performed, revealing a dramatic decrease in the amount of PRPF31 in the soluble fraction of RP11-RPE compared to isogenic control cells (Figure 1B). Notably, whilst the wild-type PRPF31 protein could be detected in the insoluble fraction of both isogenic control and RP11 RPE cells, the long mutant isoform was only detected in the insoluble fraction of RP11-RPE suggesting that a significant fraction of cytoplasmic aggregates in RP11-RPE is composed of the mutant PRPF31 (Figure 1B). The PRPF31 wild-type isoform was detected in the insoluble fraction of RP11-RPE cells. It is known that a large fraction of pre-mRNA splicing occurs cotranscriptionally in decompacted chromatin regions at the periphery or within interchromatin granule clusters, also known as nuclear speckles.[26] Nuclear speckles are enriched with splicing factors and thought to be the site for storage of spliceosomal complexes and for post-transcriptional splicing.[27][26] To examine the localisation of PRPF31 to speckles and the effect of PRPF31 mutations on the morphology of speckles, we co-stained control and RP11-RPE cells and retinal organoids with SC35 (a speckles-specific marker) and PRPF31 antibodies. Confocal microscopy revealed large nuclear speckles in control-RPE cells, where PRPF31 was localised (Figure 1C). In contrast, RP11-RPE cells showed significantly smaller nuclear speckles with reduced signal intensity, where only a small fraction of PRPF31 was localised (Figure 1C,D). Similar co-staining in retinal organoids revealed large speckles at the nuclear periphery of control photoreceptor cells, a characteristic of photoreceptor cells.[28] Notably, photoreceptor nuclear speckles significantly decreased in size in RP11-retinal organoids. Moreover, whilst wild-type PRPF31 was
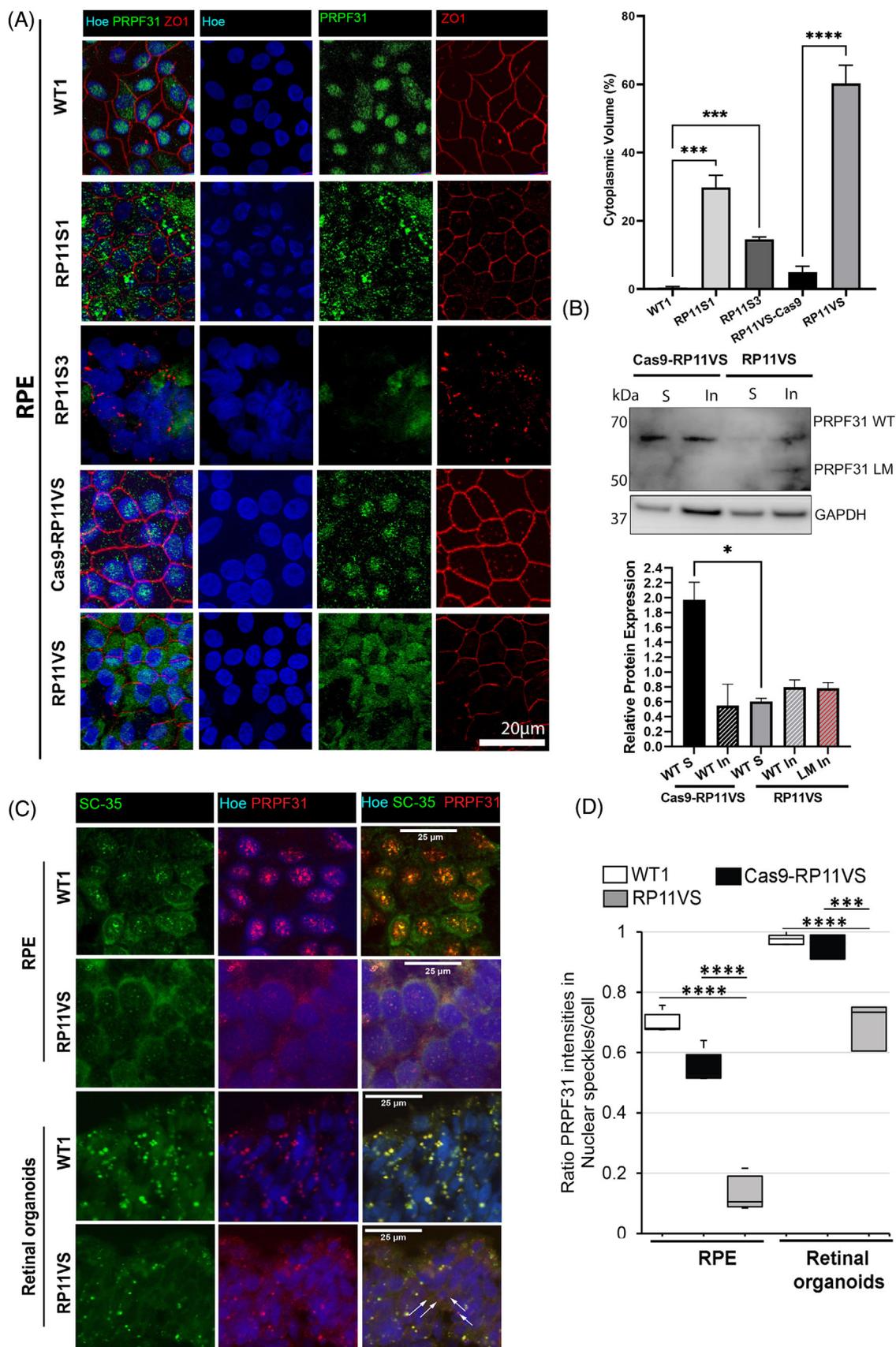
FIGURE 1 Cytoplasmic localisation of PRPF31 in patient RP11-RPE cells, altered morphology of nuclear speckles and reduced localisation of nuclear PRPF31 in splicing speckles of RP11-RPE and retinal photoreceptors. (A) Control and RP11-RPE cells were immunostained with an anti-PRPF31 N terminus (green) and ZO1 (red) antibody. Cell nuclei were stained with Hoechst.

completely localised to nuclear speckles of control photoreceptors, we noticed mislocated PRPF31 in the cytoplasm of RP11 photoreceptors (Figure 1C). Quantification of signal intensities showed that RPE was the most affected retinal cells for PRPF31 mislocalisation (Figure 1D). No difference in signal intensities was observed between the isogenic control and control RPE cells or retinal organoids.

Together our data indicate predominant cytoplasmic localisation of PRPF31 isoforms in the RP11-RPE cells, with the long mutant isoform localised in the insoluble protein fraction. Furthermore, the localisation of PRPF31 to nuclear speckles, which are essential for splicing activity, is significantly reduced in both RP11-RPE and retinal organoids.

4.1.1 | Impaired tri-snRNP assembly in Cajal bodies and reduced levels of active spliceosomes in RP11-RPE cells and retinal organoids

Since PRPF31 is an integral component of the U4/U6.U5 tri-snRNP, we next sought to analyse the effect of PRPF31 variants on the tri-snRNP formation in patient-derived retinal cells. The assembly and maturation of tri-snRNPs occur in Cajal bodies, and defects in the assembly or release of tri-snRNPs results in the accumulation of incomplete snRNPs in Cajal bodies and consequently stalling of spliceosomes at complex A.[16,29] Thus, we performed RNA-FISH using fluorescent probes against U4, U6 and U5 snRNAs followed by immunostaining for coilin, a Cajal body marker. Confocal microscopy and quantification of the fluorescent signals overlapping with Cajal bodies or the nucleoplasm revealed significant reduction of U4 and U6 levels and dramatic accumulation of U5 in Cajal bodies of RP11 photoreceptor cells compared with the controls demonstrating a defect in tri-snRNP formation in these cells (Figure 2A–D). These results are also consistent with the reduced size and intensity of nuclear speckles in RP11 retinal organoids and RPE cells. Due to very small Cajal

bodies in RPE cells, a reliable co-localisation study of snRNAs was not possible in these cells.

We next analysed formation of spliceosomal subcomplexes by fractionation of RPE and retinal organoids cell extracts on glycerol gradients (Figure 2E). Northern blotting of U snRNAs revealed increased levels of snRNAs in the top fractions[3,5] for RP11-RPE cells compared with the isogenic control (Figure S1). Notably, by comparing the snRNA profile of isogenic control RPE with that of control retinal organoids, lower amounts of tri-snRNPs in RPE cells were evident. For RP11 retinal organoids, we failed to obtain a reasonable quality of snRNA signals on Northern blots, presumably due to high RNA degradation in the sample that could not be suppressed. Western blotting of even gradient fractions of RPE cells for tri-snRNP proteins PRPF31, PRPF8 and Snu114 showed a significant increase for slow sedimenting PRPF31 in the top fractions[4,6] and altered sedimentation pattern of PRPF31-containing spliceosomal complexes in the bottom fractions (Figure 2E,F). Importantly, a band corresponding to the PRPF31 long mutant form was detected in fraction 4 of the RP11-RPE indicating that the mutant protein is not integrated into the spliceosomal snRNPs, and thus the mutant PRPF31 cannot directly perturb splicing by inhibition of spliceosome assembly (Figure 2E).

To examine the effect of defects in tri-snRNP assembly and changes in the morphology of nuclear speckles on the formation of active spliceosomes in RP11 cells, we next stained RPE and retinal organoids with an anti-phosphorylated SF3B1 antibody. The U2-specific protein SF3B1 is phosphorylated in activated (B^{act}) or catalytically active (complex C) spliceosomes, thus can be used as a marker for detection of active spliceosomes.[26] Control retinal organoids displayed large foci enriched with p-SF3B1 indicative of the sites of active splicing in photoreceptor cells (Figure 2G). These foci were prominently reduced in both size and signal intensity in RP11 organoids demonstrating reduced splicing activity in patient RP11 photoreceptors. We also stained RPE cells with p-SF3B1 antibody

---

Immunofluorescence analysis showed localisation of PRPF31 protein mainly in the nucleus of control RPE cells in speckle-like structures, whereas in RP11-RPE cells, PRPF31 protein was predominantly located in the cytoplasm in an aggregate- like pattern. Scale bars: 20 μm. Quantification of cytoplasmic PRPF31 volume showed a significant increase in the percentage of cytoplasmic PRPF31 in RP11-RPE compared to control cells. Data represent the mean ± SEM ($n = 3$). Statistical significance was assessed using one-way ANOVA. ***$P < 0.001$ ****$P < 0.0001$. (B) Representative Western blot and quantification analysis showing the expression of wild type (WT) and long mutant (LM) PRPF31 protein in the soluble and insoluble fractions of isogenic control and RP11-RPE cells. The PRPF31 N terminal antibody was used. GAPDH was used as a loading control. Data represent the mean ± SEM ($n = 3$). Statistical significance was assessed using one-way ANOVA. *$P < 0.05$. (C) Co-staining of RPE and retinal organoids with SC35 (SRSF2), a marker for nuclear speckles, and PRPF31 showing altered morphology of nuclear speckles and localisation of PRPF31 in RP11VS RPE and photoreceptor cells. Cell nuclei were counterstained with Hoechst. Arrows indicate accumulation of mislocalised PRPF31 in the cytoplasm of retinal photoreceptors. Scale bars: 25 μm. Representative images of control and RP11VS from three independent experiments are shown. (D) Quantification of signal intensities showing that PRPF31 mislocalisation is more prominent in RP11-RPE cells. A total of 200–300 cells per experiment and three independent experiments were measured and plotted. The significance was analysed by t-test; ***$P < 0.001$, ****$P < 0.0001$.
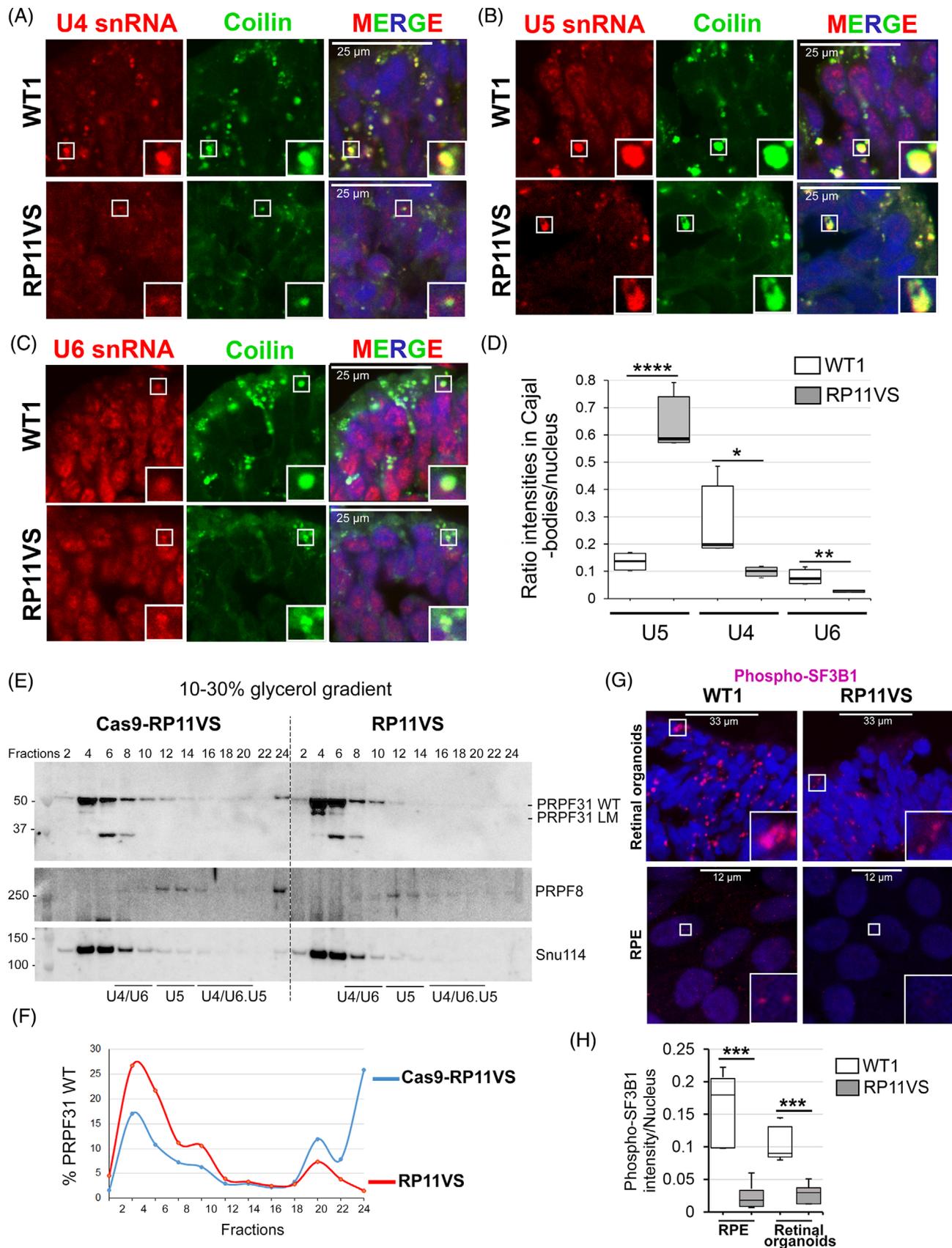
FIGURE 2 PRPF31 RP mutations lead to defects in the assembly of tri-snRNPs in Cajal bodies, and reduce formation of active spliceosomes (B[act], C complexes) in RPE and photoreceptor cells. (A–C) Confocal microscopy analyses of RNA-FISH labelling for U4 (A), U5 (B), and U6 (C) snRNAs (red) in Cajal bodies (anti-coilin, green) in control and RP11VS retinal organoids. (D) Quantification of the mean

and detected a decrease for p-SF3B1 staining in RP11-RPE compared with the isogenic control cells (Figure 2G,H).

Altogether, these results show impaired assembly of tri-snRNPs in Cajal bodies of RP11 retinal cells leading to the reduced amounts of active spliceosomes. Furthermore, the mutant PRPF31 protein does not incorporate into snRNP complexes in the nucleus and consequently cannot directly disrupt splicing, but its prominent aggregation in the cytoplasm concomitant with the reduction of wild-type PRPF31 in the nucleus leads to tri-snRNP assembly defects. This in turn can have global impact on the splicing of genes essential for the structure and function of retinal and RPE cells.

4.1.2 | Quantitative proteomics reveals major pathways affected in patient RP11 retinal organoids and RPE cells

(a) RPE cells

To identify the difference in translational profiles between RP11 patient cells and unaffected controls, high-throughput quantitative proteomics by TMT-labelling of peptides extracted from each cell line and mass spectrometry analysis was performed. RPE cells derived from control (WT1, Cas9-RP11VS) and RP11 patients (RP11S1, RP11S3, RP11VS) identified a total of 5310 proteins of which 1304 proteins were DE after applying a LFC cut-off of $\pm$ 0.5 (Table S2). GO enrichment analyses revealed amongst others enrichment of the DE proteins in RNA splicing, the spliceosome complex, retinoid metabolic process and visual perception, lysosome and protein folding pathways (Table S2). Of the 90 DE proteins in the RNA splicing pathway, fused in sarcoma (FUS) was the most downregulated protein (Figure 3A). Western blot and IF analysis corroborated these results and moreover showed that FUS was predominantly localised in the cytoplasm of RP11-RPE in an aggregate-like pattern, unlike isogenic control cells where expression was nuclear (Figure 3B,C). The mislocalisation of FUS from the nucleus to the cytoplasm has been reported previously by other studies and it has been associated with amyotrophic lateral sclerosis (ALS).[30]

Nineteen proteins involved in visual perception and 18 proteins in the retinoid metabolic pathway were DE, and

of these one the most upregulated protein was RLBP1, a protein up-regulated with age in RPE cells[31] and associated with a range of retinal dystrophies including non-syndromic autosomal recessive RP[32] and Newfoundland rod-cone dystrophy[33] (Figure 3A, Table S2). RLBP1 is a soluble retinoid carrier, which plays an important role in the regeneration of 11-*cis*-retinol during the visual cycle.[34] The upregulation of RLBP1 protein in RP11-RPE cells was further confirmed by Western blotting and by IF analysis, showing accumulation of RLBP1 in aggregate-like pattern (Figure 3B,C). In areas containing these large aggregates, we also detected disruptions of the tight junctions as well as lack of nuclei (Figure 3C). Notably, PRPF31 was also associated with the RLBP1 immunostained aggregates in RP11-RPE cells. Upregulation of visual cycle genes in RPE cells has been associated with accumulation of retinoid by-products in the aged RPE cells.[35] These results suggest that RP11-RPE cells might develop similar features to aged RPE.
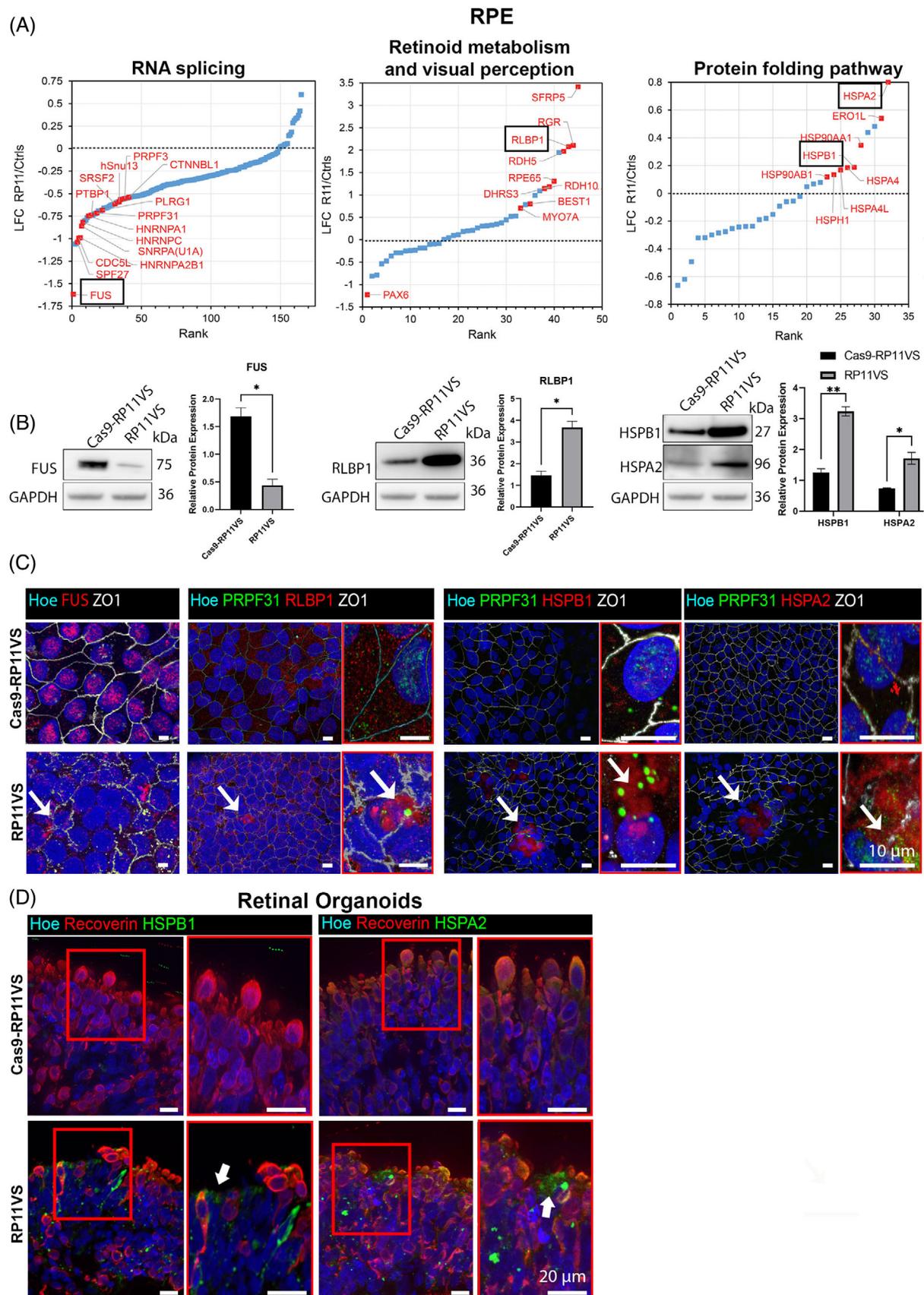
Twenty-three DE proteins were enriched in the protein folding pathway (Table S2). Moreover, two molecular chaperones involved in the UPR pathway (Figure 3A), namely HSPB1 and HSPA2 which are activated in response to misfolded proteins to restore protein conformation and to prevent protein aggregation, were upregulated in RP11-RPE cells (Figure 3A). Upregulation of HSPs in RP11-RPE cells was confirmed by Western blotting (Figure 3B), and thereafter by IF analysis (Figure 3C), demonstrating HSPB1 and HSPA2 expression in an aggregate-like pattern predominantly located in areas lacking nuclei and characterised by disrupted ZO1 staining (Figure 3C). Strikingly and in accordance with results obtained in RPE cells, we also noticed the presence of aggregate-like structures of HSPB1 and HSPA2 between patient RP11 photoreceptors (Figure 3D), suggesting a similar mechanism of protein misfolding and UPR activation in RP11-photoreceptors.

(b) *Retinal organoids*

Quantitative proteomics of retinal organoids differentiated from control (Cas9-RP11VS, WT2 and WT3) were compared to RP11-retinal organoids (RP11VS, RP11S1, RP11M and RP11S2),[10] resulting in identification of 7446 proteins, of which 1596 proteins were DE after applying a

FIGURE 3 GO analysis reveals enrichment of proteins involved in RNA splicing, retinoid metabolism and visual perception, and protein folding pathway in RP11-RPE cells. (A) GO analysis shows DE proteins involved in RNA splicing, retinoid metabolism and visual perception, and in protein folding pathway, highlighting with black circle FUS protein, which is the most downregulated protein in RP11-RPE cells from the RNA splicing pathway, RLBP1, and two HSPs; HSPB1, HSPA2. (B) Representative Western blots and quantification analysis

LFC cut-off of ± 0.5 (Table S3). GO enrichment analyses revealed an enrichment for proteins involved in several pathways; however, in view of PRPF31 aggregation in the cytoplasm and main function of photoreceptors in light transduction we focused on proteins involved in endoplasmic reticulum (ER) lumen, autophagy and lysosome, retinoid metabolism and visual perception, response to ER stress and UPR.

Since PRPF31 is a core splicing factor, we first analysed changes for proteins of the RNA splicing pathway. A total of 258 splicing proteins were identified (Figure 4A, Table S3), among which PRPF31 itself (Figure 4A,C) and several nuclear ribonucleoproteins (hnRNPD, hnRNPK, hnRNPL and hnRNPR) showed mild to strong downregulation. HnRNPs play role in multiple aspects of nucleic acid metabolism regarding transcription, alternative splicing, mRNA stability, transportation, and translation,[36,37] and their reduced expression indicates that various aspects of mRNA metabolism in RP11 organoids are disrupted from transcription to maturation, translation, and turnover. The most downregulated splicing factors in RP11 retinal organoids were NOVA1 and PTB2, which function as splicing repressors and activators.[38] NOVA1 and PTBP2 are highly expressed in the brain and involved in neuron-specific alternative splicing.[39] Since retina is part of the central nervous system, the significant downregulation of NOVA1 and PTBP2 may imply an important role for these splicing factors that deserves further investigation in the pathogenesis of RP11.

GO cellular compartment (GOCC) enrichment analysis also identified 12 DE proteins in the autophagy pathway (Figure 4B, Table S3). Autophagy is a lysosomal degradation process for the clearance of damaged organelles and unfolded proteins to maintain cellular homeostasis. Dynamic membrane trafficking events are essential for autophagy, thus vesicular trafficking proteins, Rab GTPases play important roles in various steps of autophagy process including vesicular formation, transport, tethering and fusion.[40] Interestingly, Rab27a and Rab38 levels show more than a 3-fold increase in RP11

organoids (Figure 4B, Table S3). The elevated levels of these proteins in unprenylated form have been implicated in choroidermia, a retinal degeneration disease leading to blindness in late adulthood.[41] The upregulation of additional RAB proteins (e.g., Rab1A, Rab1B, Rab12, Rab33B, Rab23) in the RP11-retinal organoids suggests an enhanced vesicular trafficking and the stimulation of autophagy.

GOCC-enrichment analysis identified 142 DE proteins associated with the lysosome as one of the most enriched compartments, with most of the proteins in this pathway being significantly upregulated (Table S3). Amongst these proteins, increased expression of two lysosomal-associated membrane proteins LAMP-1 and LAMP-2 in the RP11-retinal organoids was also confirmed by Western blotting (Figure 4C). LAMP-1 and LAMP-2 are key components of the lysosomal membrane that account for around 50% of all the proteins.[42] These two proteins facilitate the lysosomes–autophagosome fusion process,[43,44] and their upregulation in RP11-retinal organoids could signal an expansion of the lysosomal complex that is needed to cope with autophagic clearance of mis-spliced and/or misfolded proteins ensuing from the global spliceosome dysregulation.[10] In accordance with autophagy dysregulation, GOCC enrichment analysis identified 100 DE proteins localised to the ER lumen as one of the most significantly enriched compartments (Figure 4D, Table S3), including DNAJB9, DNAJC3, P4HB, HSPA5, as well as EDEM3 and ERLEC1 involved in ER-associated degradation. Notably, most of these DE proteins showed a trend for upregulation, and THBS1 involved in ER stress response was the most upregulated protein, suggesting an elevated UPR activity in RP11-retinal organoids. Consistently with this, GO biological processes (GOBP) enrichment analysis by Metascape further identified 26 DE proteins in the UPR pathway (Table S3, Figure 4E). Together these data suggest that *PRPF31* mutation-induced splicing defects may promote protein misfolding (including PRPF31 itself), resulting in activation of UPR and recruitment of heat shock proteins to the aggregates.

showing downregulation of FUS and upregulation of RLBP1, HSPB1, HSPA2 in RP11VS RPE cells. GAPDH was used as a loading control. Data represent the mean $\pm$ SEM ($n = 3$). Statistical significance was assessed using. *$P < 0.05$, **$P < 0.001$. (C) Immunostaining of RP11VS and isogenic control RPE cells with FUS (red), RLBP1 (red), HSPB1 (red) and HSPA2 (red). ZO1 (white) was used to define the tight junctions of RPE cells. Fus is located in the cytoplasm of RP11VS RPE cells (white arrow), whereas, in isogenic control RPE cells, Fus is expressed in the nucleus. RLBP1 and HSPs (HSPB1 and HSPA2) are accumulated in the cytoplasm of RP11VS RPE cells in the form of aggregates (shown by white arrow) but not in control RPE cells. Magnified images show the PRPF31 immunostaining (shown by white arrow) in RLBP1 and HSPB1 and HSPA2 aggregates (shown by white arrow). Cell nuclei were counterstained with Hoechst. Scale bars: 10 μm. Representative images from three independent experiments in RPE cells at week 12 of differentiation are shown. (D) Aggregation of HSPs in RP11VS retinal organoids. Co-staining of isogenic and RP11VS retinal organoids with HSPB1 (green) or HSPA2 (green) with Recoverin (red) showing aggregation of HSPs between Recoverin positive cells. Magnified images show co-localisation of HSPs with Recoverin in an aggregate-like form in RP11VS retinal organoids only (shown by white arrows). Cell nuclei were counterstained with Hoechst. Scale bars: 20 μm. Representative images from three independent experiments in retinal organoids day 210 of differentiation are shown.
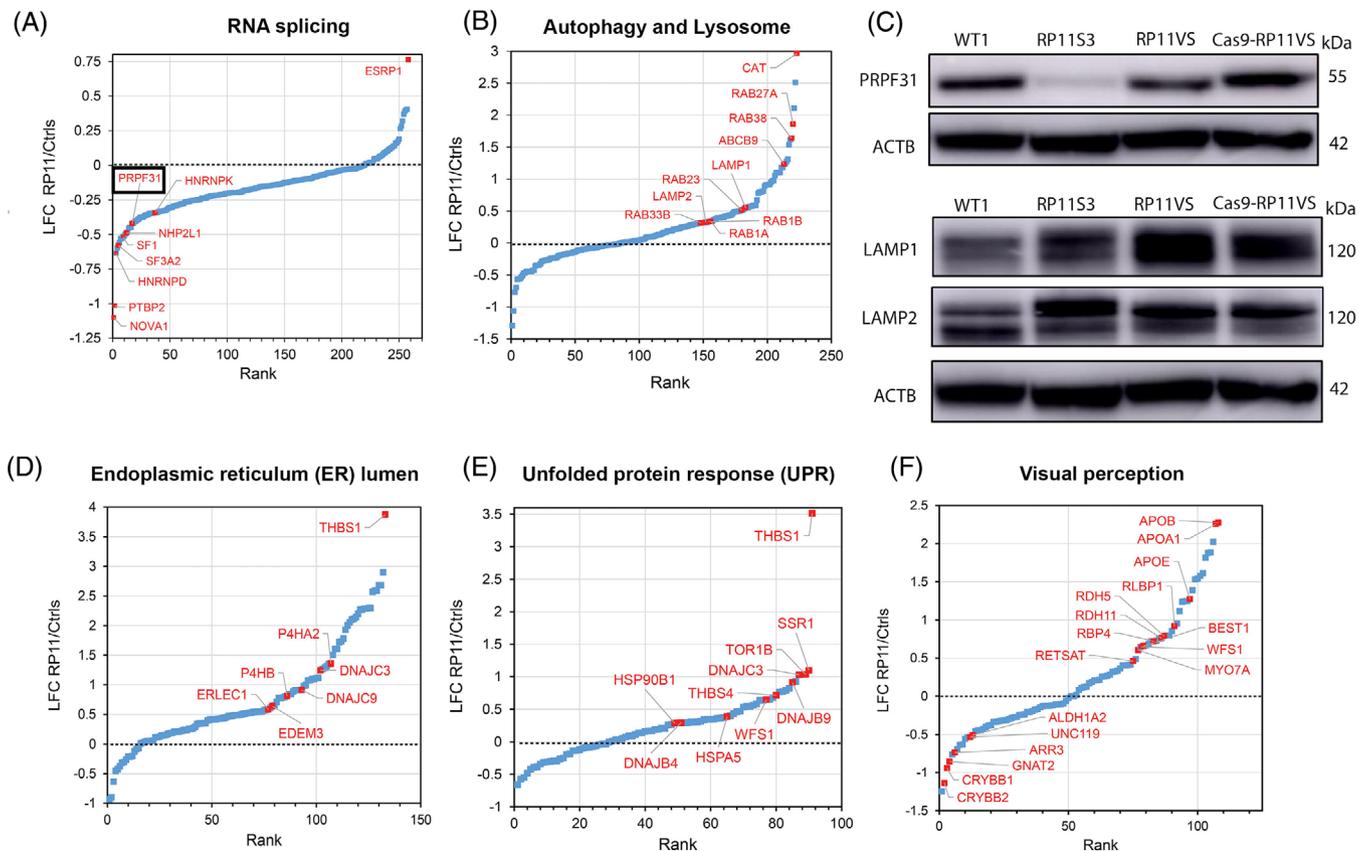
FIGURE 4 GO analysis reveals enrichment of proteins involved in RNA splicing, autophagy and lysosome, endoplasmic reticulum lumen and unfolded protein response and visual perception pathway in RP11-retinal organoids. (A) GO analysis showing DE proteins between control and RP11 retinal organoids involved in RNA splicing, highlighting with black circle PRPF31 protein. (B) GO analysis showing DE proteins between control and RP11 retinal organoids involved in autophagy and lysosome. (C) Western blot showing the downregulation of PRPF31 protein in RP11 retinal organoids compared to unaffected (WT1) and isogenic control organoids. Western blot showing upregulation of LAMP1 and LAMP2 in RP11 retinal organoids compared to unaffected (WT1) and isogenic control organoids. Representative images from three independent experiments in retinal organoids at day 150 of differentiation are shown. ACTB was used as a loading control. GO analysis identifies DE proteins between RP11-retinal and control organoids belonging to the (D) endoplasmic reticulum lumen, (E) unfolded protein response and (F) visual perception.

GOBP enrichment analysis identified 31 DE proteins involved in visual perception as one of the most enriched compartments (Figure 4F, Table S3) including RLBP1, RDH11 and RDH5, which are important proteins involved in the generation of the visual pigment and hence the maintenance of vision. Dysregulated expression of proteins involved in the visual cycle suggests changes in retinoid by-products in retinal organoids, which have been associated with retinal degeneration[35] and deserve further investigations.

4.1.3 | Proteomic analysis of cytoplasmic aggregates found in RP11-RPE cells

Our studies have shown the presence of wild type and mutant PRPF31 in the insoluble aggregates of RP11-RPE cells (Figure 1B). To assess in detail the composition of

the insoluble fraction, we performed comparative proteomic analysis of the insoluble fractions prepared from isogenic control and RP11-RPE cells separated by SDS-PAGE and analysed by mass spectrometry. Proteomic analysis detected a total of 4061 proteins, of which 934 were DE in patient RP11-RPE cells (LFC cut-off value of 1) (Figure 5A, Table S4). A comparative analysis shows that 19.4% of the total DE proteins identified in the cellular extract fraction fall into the insoluble category (Figure 5B), including proteins belonging to the visual cycle (RLBP1, DHRS3), protein folding (HSPB1) and splicing (PRPF31). Furthermore, GOBP-enrichment analysis performed by Metascape showed that the 934 DE proteins were involved in several key pathways including mRNA splicing, protein folding, response to ER stress and UPR (Figure 5C), some of which we showed earlier to be affected in RP11-RPE cells. Notably, several key spliceosomal tri-snRNP proteins including PRPF8, SNRNP200 (Brr2), PRPF4 and

(A)

(B)

Total DE proteins   Insoluble DE proteins

(C)
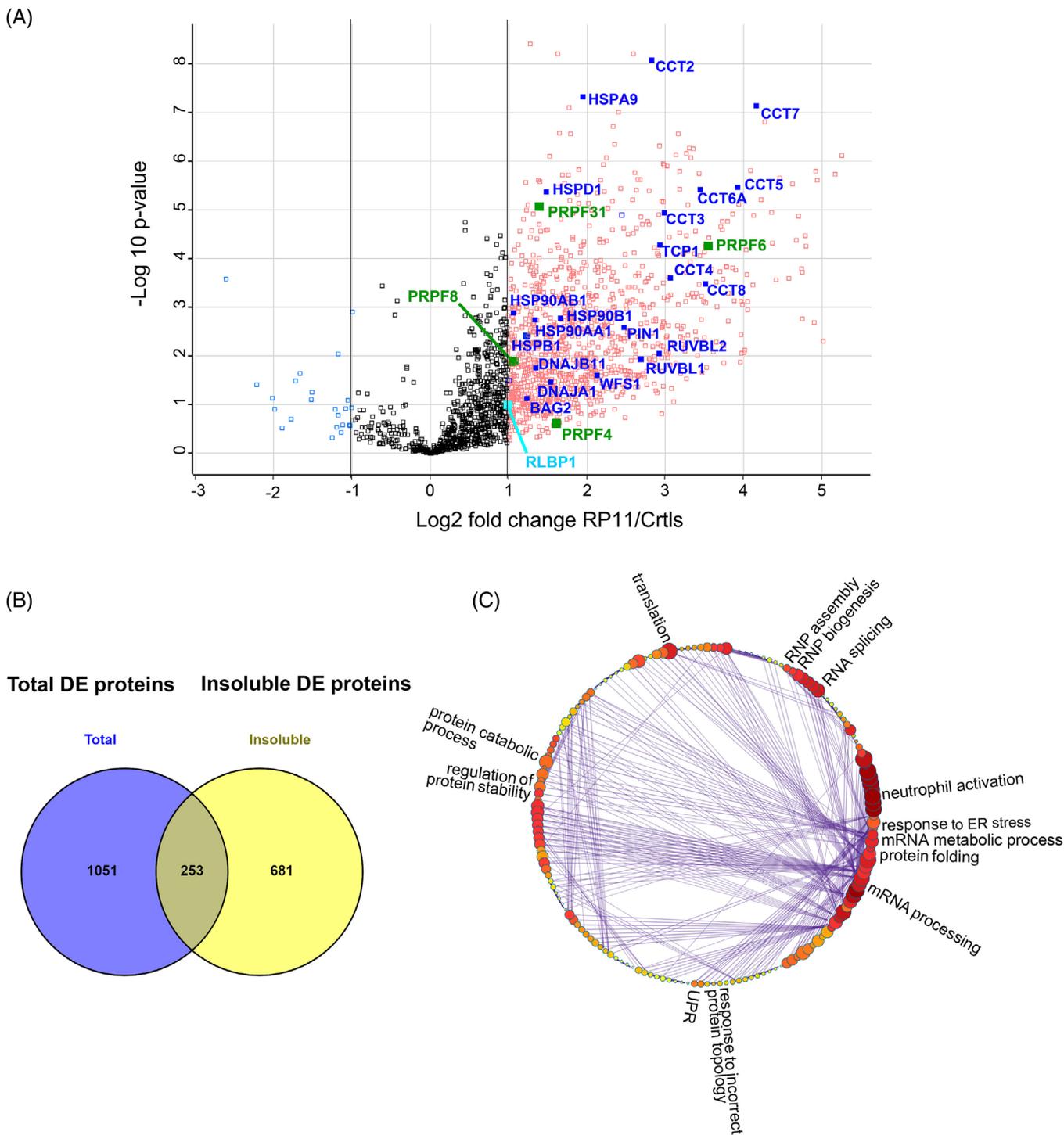
FIGURE 5 Differential protein abundance in the insoluble fractions of RP11-RPE cells. (A) Volcano plot indicating the DE proteins in the insoluble fractions of RP11-RPE cells highlighting unfolded protein response (blue), visual perception (cyan) and tri-snRNP related (green) proteins. (B) Venn diagram showing overlapping proteins between DE proteins detected from total cell extract (purple) and insoluble fractions (yellow) of RP11-RPE cells. (C) Cluster illustrating the affected pathways of enriched GOBP insoluble proteins including RNA splicing, mRNA processing, mRNA metabolic process, protein folding, UPR, regulation of protein stability, protein catabolic process, translation and RNP assembly and biogenesis. A Log2 fold change cut-off 1 was applied for the identification of significantly regulated proteins between insoluble fractions of control and RP11-RPE cells shown in Table S4.

PRPF6, implicated in RP, as well as EFTUD2 (Snu114), USP39, SART1 and SART3 were amongst the splicing factors, whose amounts were significantly increased in the insoluble fraction (Figure 5A, Table S4). Moreover, the abundance of several HSPs is notably increased including components of the HSP90/R2TP chaperone system (HSP90, RUVBL1 and 2), previously implicated in the assembly of U4 and U5 snRNPs.[45] Together these data suggest that key components of mRNA splicing, waste disposal, ER stress/UPR are deposited within the insoluble aggregates, preventing proper functions of these vital processes in RP11-RPE cells.

4.1.4 | Accumulation of misfolded protein in RP11-RPE cells

Misfolded proteins, which are unable to regain their normal conformation, are degraded by the ubiquitin-26S proteasome system.[46] For the recognition of misfolded proteins by the 26S proteasome, misfolded protein need to be tagged by ubiquitin (mono-ubiquitination) or a chain of ubiquitin polypeptides (poly-ubiquitination).[47] Given that the GO analysis showed the enrichment of proteins involved in protein folding and proteolysis in RP11-RPE cells, we used the FK1 antibody that detects ubiquitin molecules, to identify ubiquitin-conjugated misfolded proteins. Western Blot analysis show an increased abundance of ubiquitin-conjugated proteins in RP11-RPE compared to the isogenic control cells (Figure 6A). The Western blot results were further validated by IF analysis, which revealed an increased expression of ubiquitin-conjugated proteins in an aggregate-like pattern in patient-specific RP11-RPE cells, but not in isogenic control cells (Figure 6B). These FK1 positive large aggregates were found in areas with disrupted tight junctions (ZO-1 staining) and devoid of nuclei. Furthermore, PRPF31 itself was associated with these FK1 positive aggregates (Figure 6B). These results suggest that misfolded proteins destined for degradation are accumulated in the form of aggregates in RP11-RPE but not in isogenic control RPE cells, which suggests some dysfunction in the proteasome mediated degradation system in patient-specific RP11-RPE cells.

To validate the presence of cytoplasmic aggregates in RP11-RPE cells, transmission electron microscopy (TEM) analysis was performed revealing striking differences between isogenic control and RP11-RPE cells (Figure S2). Isogenic control RPE cells were characterised by normal cuboidal morphology, with no visible signs of degeneration. However, RP11-RPE cells were characterised by the presence of multivesicular bodies (MVBs, indicated by red arrowheads) as well as big vacuoles filled with electrodense material suggesting the accumulation of cytoplas-

mic aggregates. Additionally, big gaps between RP11-RPE cells filled with debris (black arrowheads) were detected (denoted by red dotted lines) suggesting the accumulation of aggregates between RP11-RPE cells and disruption of tight junctions. Additionally, TEM images revealed the presence of expanded ER (red arrows), and the presence of stress vacuoles in RP11-RPE cells (Figure S2).

4.1.5 | Dysfunction of the waste disposal mechanisms in RP11-RPE cells

In all tissues, the initial cellular defence mechanism is the ubiquitin proteasomal degradation pathway which together with the chaperone system degrades the majority of misfolded proteins.[14] Degradation of the proteins occurs in the central 20S catalytic chamber which is composed of numerous subunits, although proteolytic activities are specifically performed by $\beta 1$, $\beta 2$, $\beta 5$ subunits, which have caspase-like, trypsin-like, and chymotrypsin-like specificities.[48] Our quantitative proteomic analysis revealed the downregulation of proteins responsible for the enzymatic activities of chymotrypsin-like (PSMB8), caspase-like (PSMB9) and trypsin-like (PSMB10) in RP11-RPE cells compared to the control cells (Table S2). To validate these results, Western blot was performed using an antibody to the PSMB10 protein (involved in trypsin-like activity), which was the most downregulated proteasomal related protein (mean LFC = -0.656). The results confirmed the downregulation of PSMB10 protein in RP11-RPE compared to control cells (Figure 6C). Thereafter, the trypsin-like activity was further evaluated showing a significant decrease in the activity in RP11-RPE compared to control cells (Figure 6D). Together these results suggest a significant downregulation of the proteosome proteolytic activity in RP11-RPE cells, which may impair the clearance of misfolded proteins, leading to their accumulation in the cytoplasm of patient-specific RPE cells.

When UPR and proteasome-mediated degradation malfunction, activation of autophagy is observed.[49] To this end, we assessed the expression of key components involved at different steps (autophagosome initiation, formation and degradation) in the autophagy pathway. Our data show a significant increase in pS6, S6, p62 and LC3-II levels in RP11-RPE compared to isogenic control cells, but no differences in expression of Beclin 1 or ATG5-ATG12 (Figure 6E), suggesting a block in the late stages of the autophagy–lysosome pathway. Indeed, an accumulation of both LC3-II (autophagosome marker) and p62 (autophagy substrate) is conventionally interpreted as a block in the degradation of autophagosomes.[50] IF assays fully corroborated these data revealing accumulation of p62- and LC3-positive vesicles expression in RP11-RPE cells (Figure 6F).
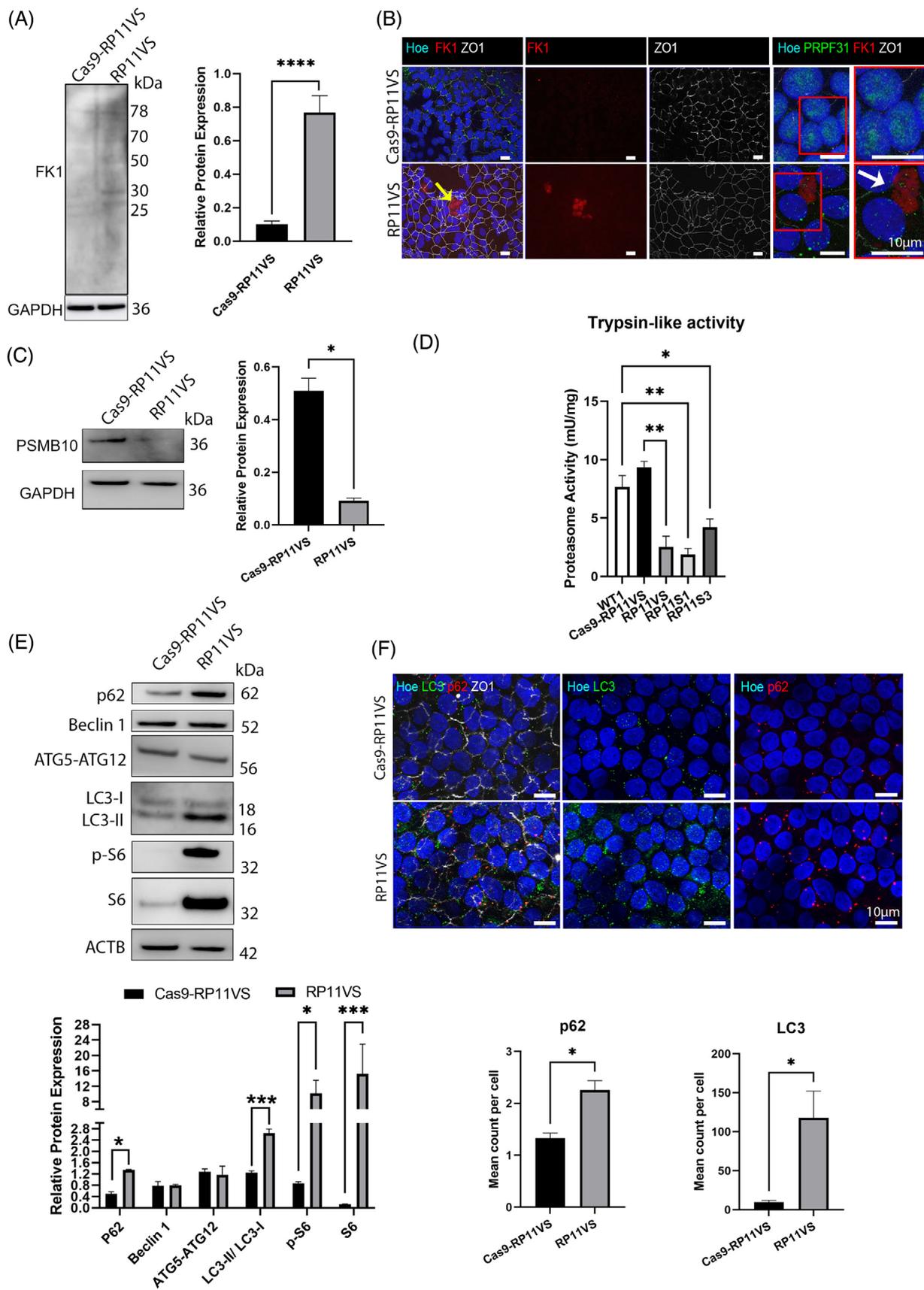
FIGURE 6 Accumulation of ubiquitin-conjugated proteins and dysfunction of the waste disposal mechanisms in RP11-RPE cells. (A) Representative Western blot and quantification analysis of all detected FK1-positive bands (ubiquitin-conjugated proteins) in RP11VS RPE cells compared to isogenic control RPE cells. GAPDH was used as a loading control. Data represent the mean ± SEM ($n = 3$). Statistical significance was assessed using unpaired Student t-test. ****$P < 0.0001$. (B) Immunostaining of RP11VS-RPE and isogenic control RPE cells

To confirm the impairment of autophagy in RP11-RPE cells, autophagy flux experiments were performed showing a significant increase in the expression of autophagy markers in the presence of Bafilomycin in the isogenic control but not patient RP11-RPE cells (Figure S3). The absence of autophagy flux therefore is likely to be responsible for the increased levels of autophagy markers in basal conditions. Interestingly, patient cells manifested with an apparent negative flux which could indicate an attempt to compensate for the absence of autophagy by the activation of another proteolytic system (Figure S3). These findings suggest the activation of the mTOR pathway and inhibition of autophagy, which together with dysfunction of the proteasome mediated degradation, may lead to accumulation of misfolded proteins in cytoplasmic-like aggregates.

4.1.6 | Progressive accumulation of cytoplasmic aggregates in RP11-RPE cells

The accumulation of aggregate-prone proteins in the intracellular space has been associated with NDs such as Alzheimer's (AD), Huntington's (HD), Parkinson's (PD), and ALS.[51][52] All these diseases are characterised by a progressive pathology leading to the death of neurons. To investigate whether this also occurs in RP11 and assess the kinetics of aggregate accumulation in RP11-RPE cells, we performed IF analysis at week 4, 8 and 12 post-plating of RPE cells in trans-wells, using antibodies to RLBP1, HSPB1 and FK1, which we showed earlier to accumulate in an aggregate-like pattern. Week 4 RP11-RPE cells displayed increased expression of RLBP1 and HSPB1 but not FKI compared to isogenic control cells (Figure 7). Further increases in the expression of RLBP1, and HSPB1 were noticeable in RP11-RPE cells assessed at week 8 (Figure 7). FK1 expression was also increased at week 8 and RLBP1 was the only protein that showed accumulation in an aggregate-like pattern. At 12 weeks, all three markers displayed an increased expression in an aggregate-like pattern, but only in the patient RP11-RPE cells, corroborating our earlier data (Figure 7). These results suggest a progressive accumulation of visual cycle proteins, chaperones and misfolded-ubiquitinated proteins in the cytoplasm of RP11-RPE cells.

4.1.7 | Daily feeding of RP11-RPE cells with POSs accelerates cytoplasmic aggregate accumulation

One of the main functions of RPE cells is the engulfment and phagocytosis of POSs, which are shed from photoreceptors daily at a very high rate. To assess the aggregate accumulation under physiologically relevant conditions, the control and RP11-RPE cells differentiated in trans-wells for 4 weeks, were fed with unlabelled POSs, and collected at 0, 48, 96 and 144 h post-feeding. Thereafter, the presence of intracellular aggregates containing RLBP1, HSPB1 and/or FK1 was analysed by IF microscopy (Figure S4A, S5). To ensure cellular uptake, FITC-labelled POSs were used in additional experiments (Figure S4A, B). RP11-RPE cells fed with POSs at 0 h, did not show any differences in RLBP1, HSPB1 or FK1 expression compared to isogenic control RPE cells. However, at 48 h post-feeding with POSs, RP11-RPE cells showed a significant increase in the accumulation of cytoplasmic aggregates containing RLBP1, HSPB1 or FK1, compared to isogenic control cells (Figure S4A,B, S5A–C). A further accumulation of proteins was observed at 96 and/or 144 h post-feeding, with RLBP1, HSPB1 and FK1 expressed as large aggregates in the cytoplasm of RPE cells disrupting the tight junctions between the cells (Figure S4A,B, S5A–C); this however was not observed in the isogenic control RPE cells. Additionally, the expression of LC3 and p62 was assessed, showing a gradual increase in the expression with time post-POSs feeding (Figure S4A,B, S5D,E), but only in the RP11-RPE cells. Interestingly, FITC-labelled POSs accumulated in a large-aggregate like pattern in RP11VS-RPE

---

with FK1 (red) and ZO1 (white) showing accumulation of FK1 in RP11VS-RPE cells in the form of aggregates (shown by yellow arrow) but not in control cells. Magnified images show association of FK1 with PRPF31 (shown by white arrow). Cell nuclei were counterstained with Hoechst. Representative images from three independent experiments in RPE cells at week 12 of differentiation are shown. Scale bars: 10 μm. Data obtained from RPE cells at week 12 of differentiation. (C) Representative Western blot and quantification analysis of RPE samples showing downregulation of PSMB10 protein in RP11VS RPE cells compared to isogenic control. GAPDH was used as a loading control. Data represent the mean $\pm$ SEM ($n = 3$). Statistical significance was assessed using. *$P < 0.05$. (D) Reduced Proteasome Trypsin-like activity in RP11-RPE compared to control RPE cells. Statistically significant differences are determined by one-way ANOVA (*$P < 0.05$, **$P < 0.001$). Data are presented as mean $\pm$ SD, $n = 3$. (E) Representative Western blot and quantification analysis of key autophagic components showing upregulation of p62, LC3-I, LC3-II, p-S6 and S6 expression in RP11-RPE cells compared to isogenic control RPE cells. Actin B was used as a loading control. Data represent the mean $\pm$ SEM ($n = 3$). Statistical significance was assessed using two-way ANOVA. *$P < 0.05$, ***$P < 0.001$. (F) Quantitative immunofluorescence analysis showed upregulation of p62 (red) and LC3 (green) in RP11VScompared to isogenic control RPE cells. ZO1 (white) was used to define the tight junctions of RPE cells. Cell nuclei were counterstained with Hoechst. Scale bars: 10 μm. Statistically significant differences are indicated by paired Student t-test,*$P < 0.01$. Data are presented as mean $\pm$ SEM, $n = 5$.
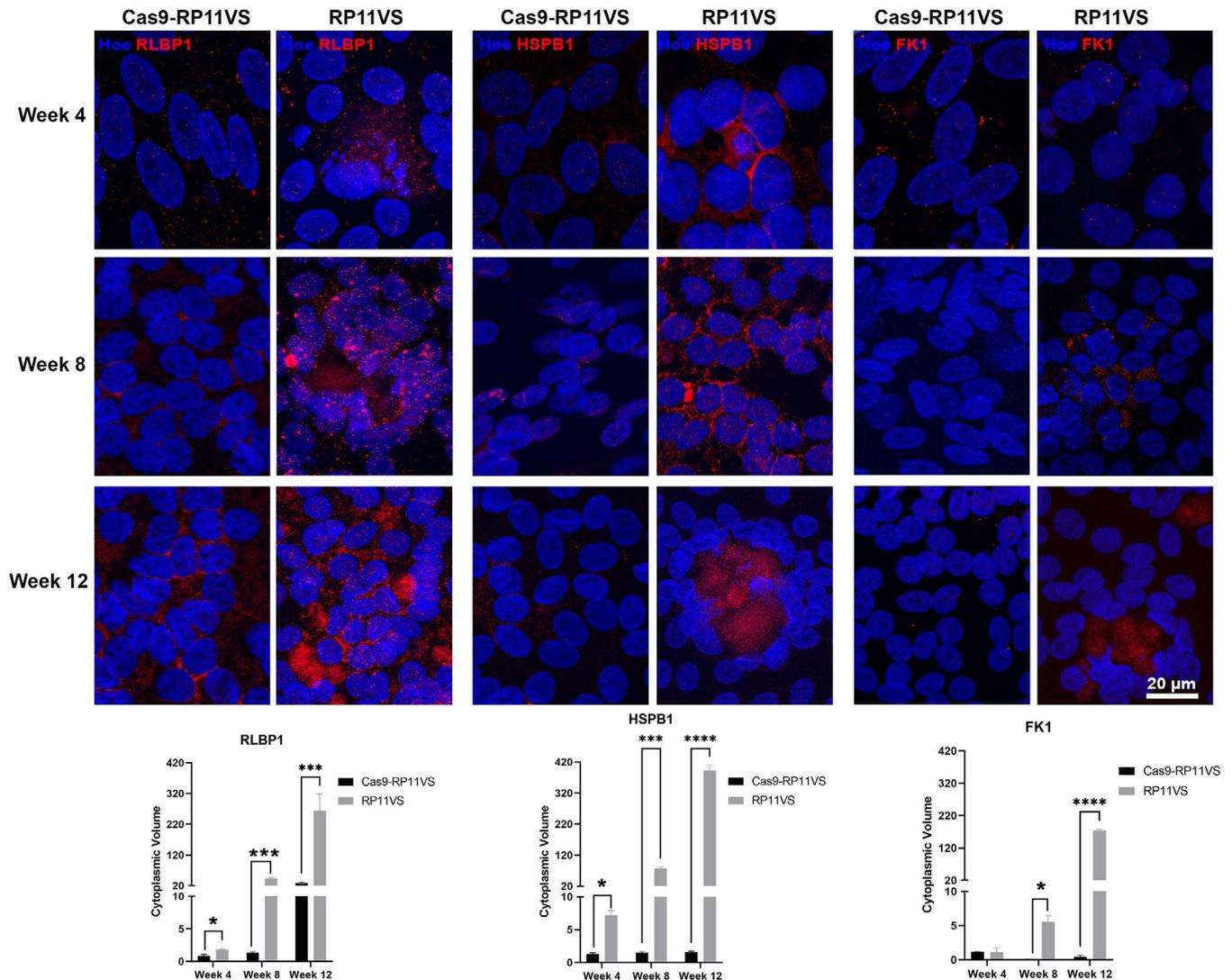
FIGURE 7 Progressive accumulation of cytoplasmic aggregates in RP11-RPE cells. Representative immunofluorescent images and quantification analysis of isogenic control and RP11VS RPE cells at week 4, 8 and 12 showing a gradual increase and accumulation of RLBP1, HSPB1 and FK1 (red), forming large aggregates. Cell nuclei were counterstained with Hoechst. Scale bars: 20 μm. Data represent the mean $\pm$ SEM ($n = 3$). Statistical significance was assessed using unpaired Student t-test. *$P < 0.05$, ***$P < 0.001$ ****$P < 0.0001$.

cells, but not control cells at 144 h post-feeding (Figure S4A, B). Under normal steady-state conditions, cytoplasmic aggregates should be digested by the autophagy or proteasome mediated degradation; however, the accumulation of p62 and LC3 observed only in RP11-RPE cells suggests that the waste disposal mechanism is impaired or overwhelmed, resulting in aggregate accumulation. Altogether these results suggest that daily feeding of RP11-RPE cells with POSs accelerates the accumulation of cytoplasmic aggregates containing amongst others RLBP1, FK1 and HSPB1 proteins in RP11-RPE cells.

To assess the impact of cytoplasmic aggregate accumulation on cell survival, control and RP11-RPE cells were immunostained with a Caspase-3 antibody. Caspase-3 is synthesised as inactive proenzyme and is localised in the cytoplasm. However, during apoptosis, caspase-3 is proteolytically cleaved, activated, and translocated into the nucleus causing fragmentation of DNA and damaging essential cellular proteins including enzymes involved in DNA repair.[53] Our data show that Caspase-3 is predominantly expressed in the cytoplasm of isogenic control RPE in contrast to RP11-RPE cells, where Caspase-3 is mainly expressed in the nucleus (Figure S6A), suggesting the activation of Caspase-3 in the latter.

Collectively, our findings reveal the accumulation of cytoplasmic cellular aggregates containing amongst others both the wild-type and mutated PRPF31 isoforms, misfolded ubiquitin-conjugated, chaperones and visual cycle proteins in RP11-RPE cells. The proteasome-mediated and autophagy degradation pathways are both impaired, result-

ing in the progressive accumulation of these cytoplasmic aggregates with time. This process is exacerbated under physiological conditions, leading to disruption of tight junctions and activation of cell death through apoptosis.

4.1.8 | Elimination of aggregates in RP11-RPE cells by pharmacological drugs

To assess whether cytoplasmic aggregate accumulation could be eliminated, we tested the following pharmacological drugs:

1. Arimoclomol, an investigational drug currently in phase III of clinical trial for ALS.[54] This is a heat shock protein co-inducer that has been shown to enhance HSPs expression both in vitro[55] and in vivo[56] and to alleviate protein aggregation.
2. STF-083010, a pharmacological compound shown to decrease cell death and attenuate oxidative stress by targeting IRE1, which mediates the UPR.[57]
3. Salubrinal is another pharmacological drug that has been shown to have neuroprotective effects in ALS animal models[58,59] by blocking the PERK pathway, leading to further inhibition of the protein synthesis.[60]
4. Rapamycin, a widely used pharmacological compound able to activate autophagy by inhibiting mTORC1.[61,62]
5. Trehalose, an AMPK-dependent activator,[19,63] has been shown to activate autophagy and confer beneficial effects for the elimination of cytoplasmic aggregate-prone proteins. Compounds used in groups 1–4 were dissolved in DMSO, whilst group 5 compound was dissolved in water, hence DMSO and water groups were as vehicle controls, respectively.

Their effects on cytoplasmic aggregates were assessed following 7-day treatment of RP11-RPE cells differentiated on trans-wells for 12 weeks. Immunostaining with RLBP1, HSPB1 and FK1 was performed to detect cytoplasmic aggregates. The data showed no significant difference in the accumulation of cytoplasmic aggregates containing RLBP1, HSPB1, FK1 in RP11-RPE cells treated with Salubrinal, Arimoclomol, STF-083010 or trehalose (Figure 8A). Interestingly, a significant reduction in cytoplasmic aggregate accumulation was observed in RP11-RPE cells treated with Rapamycin only (Figure 8A). The same results were obtained in RP11-RPE cells from a second patient, harbouring the same *PRPF31* mutation (Figure S7), and a third patient with a different *PRPF31* mutation (Figure S8). Western blot analysis was performed in isogenic control and patient RPE cells to assess whether autophagy was indeed activated in RP11-RPE cells after treatment with Rapamycin, demonstrating a decrease in the expression of pS6 and S6 in the Rapamycin treated RP11-RPE cells, and an increase in the expression of LC3-II. However, no differences were detected in the expression of LAMP1 and p62. Furthermore, a decrease in the expression of RLBP1 and HSPB1 was detected after treatment of RP11VS RPE cells with Rapamycin suggesting that Rapamycin induced the activation of autophagy in RP11-RPE cells leading to a significant elimination of aggregates containing RLBP1, HSPs or FK1 in RP11-RPE cells (Figure 8B). Western blot analysis of vehicle-treated and Rapamycin-treated RP11-RPE cells was performed in the two additional patients with severe clinical phenotype, confirming the activation of autophagy and elimination of cytoplasmic aggregates (Figure S7B, S8B).

Thereafter, we assessed the effects of Rapamycin-treated RP11-RPE cells on cell survival after 7 days treatment of RP11-RPE cells with vehicle or Rapamycin, respectively. In Rapamycin-treated RP11-RPE cells, we observed reduced nuclear localisation of Caspase-3, indicating a positive effect in cell survival (Figure S6B). The reduced nuclear localisation of Caspase-3 was further confirmed by Western Blot (Figure S6C). These results suggest that Rapamycin has a positive impact in the elimination of cytoplasmic aggregates, potentially leading to enhanced cell survival.

4.1.9 | Differential expression and aggregate formation of key proteins implicated in retinitis pigmentosa

We next searched in our proteomics datasets for other retinal-specific proteins DE in PP11-RPE or retinal organoids or deposited within the aggregates. To this end, Metascape was used to retrieve DE genes associated with diseases from the DisGeNET database (Tables S2, S3, S4). This analysis revealed RP as one of the enriched disorders in both datasets of RPE and retinal organoids DE proteins.

In RPE total fraction, besides RLBP1, we found also upregulation of Bestrophin-1 (BEST1, Figure 3A), an anion channel expressed in RPE and essential for calcium signalling, whose mutations lead to RP.[59] PROS1 levels that have been linked to juvenile RP are increased within the insoluble RPE fraction.[64] Retinol dehydrogenase 5 (RDH5) previously linked to RP was significantly upregulated in the total (Figure 3A) and insoluble RPE fractions.[65] *PHYH*, whose mutations cause adult Refsum disease, a peroxisomal disorder with numerous features including RP,[66] is upregulated in the total cellular and insoluble fractions. In addition, differential expression of key RPE proteins RGR, RPE65 and MYO7A (Figure 3A) was noticed in our total RPE proteomics dataset.
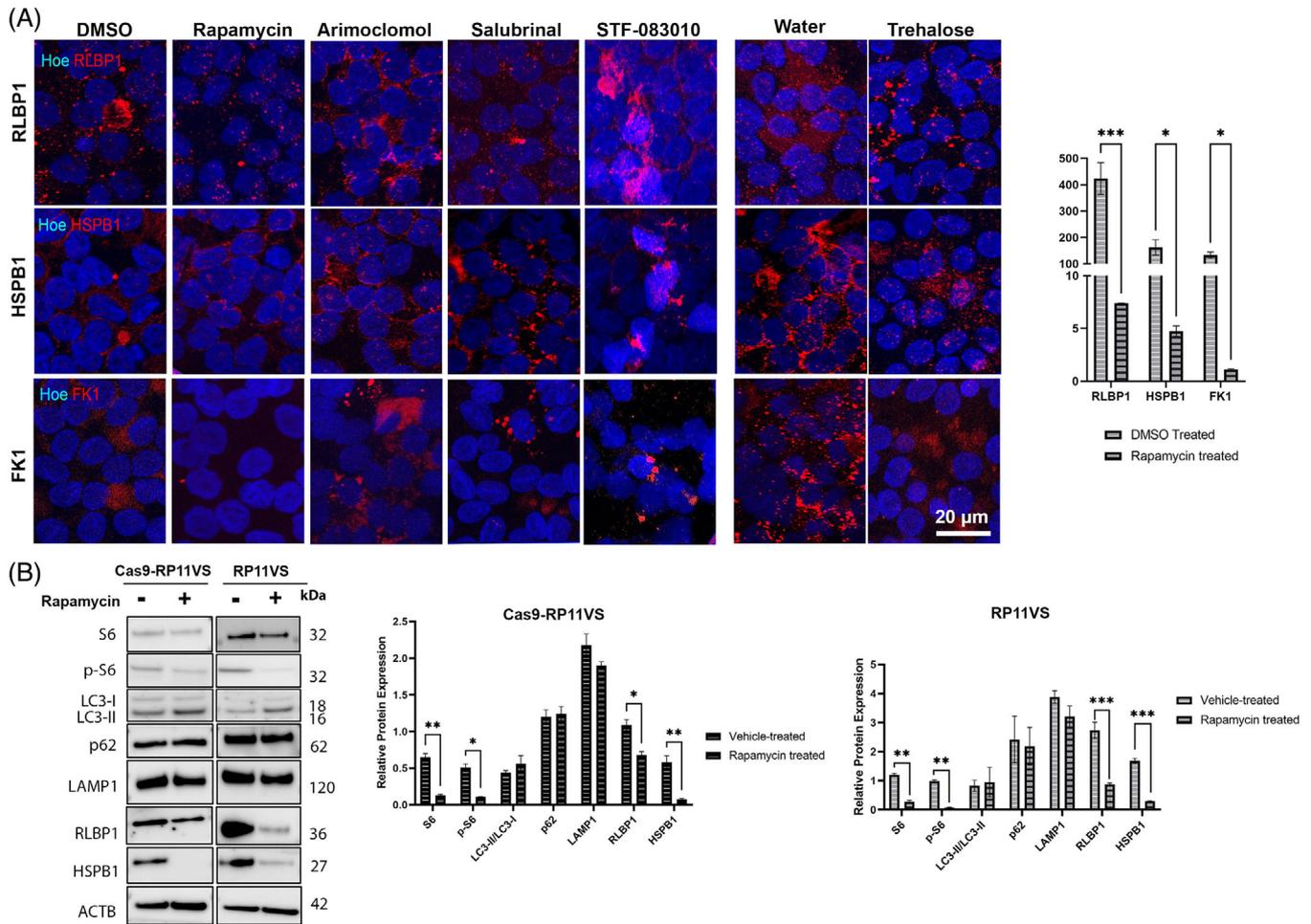
FIGURE 8 Elimination of aggregates in RP11-RPE cells through application of Rapamycin. Representative immunofluorescence images and quantification analysis of RP11VS-RPE cells showing a significant decrease of cytoplasmic aggregates containing RLBP1 (red), HSPB1(red) and FK1 (red) upon daily treatment with Rapamycin (500 nM) for 7 days. No apparent differences were observed in cytoplasmic aggregates after seven days treatment with Arimoclomol (1 μM), Salubrinal (25 μM), STF-083010 (50 μM) and trehalose (50 mM). DMSO was used as a vehicle control for Rapamycin, Arimoclomol, Salubrinal and STF-083010, and distilled water was used as vehicle control for Trehalose. Cell nuclei were counterstained with Hoechst. Scale bars: 20 μm. Quantification of these results is shown on the right-hand side graph presented as mean $\pm$ SEM ($n = 3$). Statistical significance was assessed using paired Student t-test. *$P < 0.05$, ***$P < 0.001$. (B) Western blot and quantification analysis of 7 days Rapamycin-treated isogenic control and RP11VS-RPE cells showing the decrease in the expression of S6, p-S6 RLBP1, HSPB1 and increase in LC3-II expression in RP11VS-RPE cells. Actin B was used as a loading control. Data represent the mean $\pm$ SEM ($n = 3$). Statistical significance was assessed using two-way ANOVA. *$P < 0.05$, **$P < 0.001$, ***$P < 0.001$. Please refer to Figures S7 and S8 for the same analysis in two additional RP11-RPE cells.

In retinal organoids total fraction, we detected upregulation of HGSNAT, a lysosomal acetyltransferase whose variants are the cause of RP-73, and HKDC1, a hexokinase localized to the photoreceptor inner segment and associated with autosomal recessive RP, as well as Retinol dehydrogenase 11 (RDH11) associated with syndromic RP, and the MYO7A protein (Figure 4F) involved in Usher syndrome with an RP phenotype. GNAT2, a gene associated with cone-rod dystrophies is the most significantly downregulated protein essential for the phototransduction pathway in RP11 retinal organoids (Figure 4F).[67] Together our data demonstrate dysregulation of expression and/or local-

isation and/or aggregation of multiple RP genes in both RP11-RPE cells and retinal organoids ensuing from *PRPF31* mutations.

5 | DISCUSSION

In previous work, using an iPSC-disease modelling approach, we have shown that mutations in the spliceosomal U4/U6 snRNP-specific protein PRPF31 result in global splicing changes specifically in retinal cells and RPE.[10] To fully understand the impact of such global splicing

dysregulation on the patient-derived RPE and retinal cells, we have undertaken a detailed quantitative proteomic and IF analysis, as well as biochemical analysis of these cells harbouring *PRPF31* mutations. These new findings have shown the predominant accumulation of the mutant PRPF31 protein as aggregates in the cytoplasm of RPE cells and its significant presence in the cytoplasm of retinal cells. This results in reduced nuclear levels of wild-type isoform in RP11 patient RPE and retinal cells, leading to reduced amounts of U4/U6 snRNPs and accumulation of U5 in Cajal bodies, thus defects in tri-snRNP formation as well as smaller size of nuclear speckles. These assembly defects also result in reduced amounts of active spliceosomes in both RPE cells and retinal organoids. Quantitative proteomics revealed that several key cellular processes in addition to mRNA splicing, namely waste disposal and UPR, were significantly affected resulting in progressive accumulation of insoluble aggregates containing key components of each of the pathways within RPE cells that affected cell viability. Aggregate formation also affected the expression and/or localization of key proteins of the retinoid metabolism and visual perception pathways including RLBP, which accumulated in the PRPF31 cytoplasmic aggregates. Furthermore, proteomic analysis of insoluble aggregates in RP11-RPE cells identified the presence of other core components of the tri-snRNP including PRPF6, PRPF4 and PRPF8 (all of which are linked to adRP) together with chaperone proteins important for U4/U6 and U5 snRNPs assembly. Strikingly, activating autophagy via application of Rapamycin resulted in reduction of these cytoplasmic aggregates and improved cell survival.

Aggregation of PRPFs in retinal photoreceptors and RPE cells has been reported previously and shown to be cell-type specific. For example, the mutant PRPF3[T494M] amasses in big aggregates in the nucleolus region,[11] causing mislocalisation of splicing factors that may be detrimental for photoreceptor cells. In contrast, the mutant PRPF31 protein forms insoluble aggregates in the cytoplasm of RPE cells of Prpf31[A216P/+] mice,[13] decreasing the protein levels of this splicing factor in the nucleus. Our data show reduced nuclear expression of the wild-type PRPF31 and cytoplasmic localisation of mutant PRPF31 protein, corroborating the mouse RPE cell studies. Knockdown studies in HeLa cells have demonstrated that lack of Prpf31 or Prpf6 leads to accumulation of U4/U6 di-snRNPs in Cajal bodies and inhibition of tri-snRNP formation.[17] Nonetheless, a detailed analysis of the impacts of *PRPF* mutations on tri-snRNPs formation within Cajal bodies of retinal cells, spliceosome assembly in nuclear speckles and formation of active spliceosomes directly on patient-specific RPE and retinal cells has not been reported previously. Using a combination of RNA-FISH and IF microscopy, we demonstrate a significant defect in the tri-snRNP assembly in patient photoreceptor cells leading to a decrease in U4/U6 di-snRNPs and accumulation of U5 snRNP in Cajal bodies, the nuclear membraneless organelles where tri-snRNPs are assembled and fully matured.[16] Strikingly, glycerol-gradient fractionation combined with Northern and Western blotting demonstrated for the first time that the mutant PRPF31 is not incorporated into the spliceosomal complexes in RP11-RPE cells. Moreover, an accumulation of U4 and U6 and slow sedimenting PRPF31 in the gradient top fractions are observed in the RP11-RPE cells. These defects in tri-snRNP formation in RP11 cells most likely will lead to perturbed pre-mRNA splicing. Consistently, RP11 retinal organoids and RPE cells showed altered morphology of nuclear speckles, the nuclear compartments for storage of splicing factors and associated with post-transcriptional splicing, as well as reduced localisation of PRPF31 to these compartments suggesting a reduction in active spliceosomes. To prove this, we immunostained the retinal organoids and RPE cells with an antibody raised against a phosphorylated form of the U2-specific protein SF3B1, which is phosphorylated in activated (B[act]) or catalytically active (complex C) spliceosomes. A significant reduction in staining was observed in RP11 retinal organoids, demonstrating reduced levels of active spliceosomes and splicing activity in patient cell lines. A mild reduction for p-SF3B1 staining in RP11-RPE cells was also observed, suggesting a reduced splicing activity in these cells compared to controls. Notably, gradient profiles showed lower levels of tri-snRNPs in RPE cells compared to retinal organoids, which could further imply that even mild changes in the splicing activity would impact RPE cells more significantly than retinal cells. This however needs further investigations in RP11-RPE cells as well as other PRPF-RPE cells, which is currently ongoing in our groups.

In addition to splicing dysregulation, our proteomics data revealed an enrichment of proteins involved in the retinoid metabolic process and visual perception. Of particular interest in the retinoid metabolic and visual perception is the RLBP1, which is significantly overexpressed in RP11-RPE cells, and found in the form of cytoplasmic aggregates. RLBP1 is a retinoid-binding protein expressed in RPE and Müller glia cells and involved in the conversion of 11-*trans*-retinal to the light sensitive 11-*cis* retinal.[68] Mutations in *RLBP1* cause a range of retinopathies including retinitis punctata albescens (RPA), Bothnia-type dystrophy (BD), Newfoundland rod-cone dystrophy (NFRCD), RP and fundus albipunctatus (FA).[69] Based on our data, our hypothesis is that accumulation of RLBP1 in the insoluble aggregates reduces the available RLBP1 protein needed for recycling of retinal, impacting directly on the visual cycle and the phototransduction pathway.

Studies performed in the RPE of Prpf31$^{A216P/+}$ mice have revealed overexpression of heat shock protein 70 (Hsp70) family, and its co-localisation with mutant Prpf31 in the insoluble cytoplasmic aggregates. It is reasonable to assume that protein aggregation of mutant PRPF31 is responsible for activating the chaperone response. Corroborating these studies, our data also revealed significant changes in expression of several HSPs and overexpression of HSPA4L, HSPB1 and HSPA2, that accumulated in the form of aggregates in association with PRPF31 in RP11-RPE cells. Remarkably, HSP aggregation between photoreceptor cells was also observed in RP11 retinal organoids. HSPs facilitate protein homeostasis and cell protection against damaged proteins or aggregation of harmful denatured proteins. Their upregulation in RP11-RPE cells could be a direct response of global splicing dysregulation, which is bound to result in misfolded or aggregated proteins, as shown in our study. Previous studies have reported that under stress conditions (e.g., hyperglycemia) or upon mutations, soluble HSPs are depleted, becoming unavailable to target other proteins, affecting further their functionality[70] and leading to the accumulation of insoluble aggregates in the retina.[70] Our data demonstrate preferential HSP accumulation in the insoluble aggregates of RP11-RPE cells, suggesting a change in their solubility and function, which could be due to "overwhelming" of HSP response by the large amount of misfolded or aggregates proteins resulting from the global spliceosome dysfunction.

The formation of cytoplasmic aggregates is a common hallmark event of many NDs and is associated with protein misfolding.[1] Usually, in response to misfolded protein, cellular defence mechanisms like molecular chaperons such as HSPs are activated. However, when quality control systems are incapable to restore the normal conformation of denature proteins and thus are overloaded with excessive amounts of denatured proteins, then it is possible that the solubility of HSPs can be transformed from a soluble state to an insoluble form as shown in our study. When HSPs fail to restore misfolded proteins, denatured or aggregated proteins are tagged with ubiquitin (Ub) and are directed to the Ub-proteasome system (UPS) for proteolytic degradation.[51] Our results revealed increased protein ubiquitination and a reduced enzymatic activity (trypsin-like) of the proteasome degradation system in RP11-RPE compared to control RPE cells. The reduced proteasome activity revealed in our results is also a common characteristic feature of other NDs such as AD, PD, ALS and HD.[51] Particularly in AD disease, various studies have shown that tau aggregates can bind to the recognition site of the 19S catalytic particle of the proteasome inducing protein congestion that further leads to impairment of protein degradation.[71] Also, misfolded prion proteins (β-sheet-rich PrP) in Prion disease disrupt the opening of the 20S proteasome particle, thus inhibiting the function of the 26S proteasome.[72] This association of pathogenic protein aggregates and reduced or blocked proteasome activity has been reported by several studies focusing on the AD.[73,74] Our data mirror these findings, however, in the case of RP11-RPE cells, it is unknown whether the accumulation of misfolded/aggregated proteins is a result of decreased proteasome activity or whether the proteasome system is incapable of coping with the burden of misfolded, ubiquitinated and aggregated proteins resulting from global spliceosome dysregulation.

Under stress conditions when the chaperone and proteasome systems are overwhelmed, clearance of cytoplasmic aggregates is facilitated by autophagy, where cytoplasmic substrates are engulfed and degraded into amino acids.[51] Although most proteins in the human genome can be successfully degraded from the cells, genetic defects can affect their conformation leading to the formation of aggregates. For example, mutations of huntingtin proteins inhibit the proteolytic machinery and induce accumulation of cytoplasmic aggregates in patients with HD.[75] This is characterised by an increase of key autophagic components such as p62, LC3 in HD mouse models due to the impairment of cargos to be directed to autophagic vacuoles for degradation.[76] Likewise, our results demonstrate an upregulation of p62 and LC3 expression in RP11-RPE cells compared to control RPE cells suggesting an impairment of autophagy. In the recent years, a specialised form of non-canonical autophagy namely LC3-associated phagocytosis (LAP), has been described as a key mechanism in RPE cells for degradation of POSs. It could thus be envisaged that the upregulation of LC3 expression in RP11-RPE cells could reflect activation of LAP.[77] Although many proteins are common between these two autophagy branches, two key proteins (Rubicon and Nox2), distinguish LAP from canonical autophagy. A careful examination of our proteomics data did not reveal any changes in expression of these two proteins in RP11-RPE cells. Importantly, LAP is not dependent on the AMPK/mTORC1/ULK1 axis, thus is LAP was to be inhibited instead of canonical autophagy, treatment with Rapamycin would have no impact on RP11-RPE cells, which is not the case. For these reasons, we believe that the canonical autophagy and not LAP is dysregulated in RP11-RPE cells. We further hypothesise that this combined dysfunction of proteasome and autophagy mediated degradation together with accumulation of HSPs in the insoluble fractions leads to the accumulation and growth of larger aggregated proteins, which may be cytotoxic to the cells. This is a characteristic of many NDs such as HD, AD, PD and ALS, where mutant-aggregated proteins become resistant to degradation inducing cytotoxicity and neuronal cell death.[51] To

this end, it has been reported that neuronal cells of AD patients[78] have increased levels of Caspase-3, associated with degeneration of synapses and a decrease in synaptic plasticity, suggesting that intracellular protein deposits might disrupt the normal function of neurons, inducing stress which in turn leads to the initiation of cell death. Similarly, our results have shown the progressive accumulation of large cytoplasmic aggregates containing the mutant PRPF31 itself as well as misfolded, ubiquitin conjugated, and visual cycle proteins in areas with disrupted tight junctions and increased Caspase-3 activity. Tight junction disruption has been reported by other studies associating RPE remodelling with retinal degeneration.[79] Collectively, these results suggest that continuous accumulation of aggregates in patient-specific RP11-RPE cells impairs RPE cell survival. Similarly, our previous studies showed a 150% increase in cells with apoptotic nuclei in the PRPF31 retinal organoids compared to controls.[10] In accordance, the PRPF31 retinal organoids generated in this study were significantly smaller ($p < 0.0001$, surface area PRPF31 ROs: $956.4 \pm 24.30 \ \mu m^2$ versus control ROs: $1598 \pm 54.46 \ \mu m^{2,}$ day 150): these were also characterised by the presence of cytoplasmic aggregates between the photoreceptors. Together these data suggest that aggregate related impaired survival is also occurring in the PRPF31 retinal organoids.

One potential strategy to enhance the degradation of misfolded proteins is to induce activation of autophagy. Many small molecules have been developed to activate autophagy and induce clearance of pathogenic proteins, and the most widely known is by inhibiting mTORC1 by Rapamycin. By searching in our proteomic datasets, we find components of the mTOR signalling pathway upregulated to various levels in both RPE and retinal organoids. These include PDK1, a key protein for activation of the mTOR pathway. Moreover, components of the regulator complex involved in the activation of mTORC1 (including LAMTOR1, LAMTOR2, LAMTOR4) are enriched in retinal organoids. It has been shown that Rapamycin can effectively reduce cytoplasmic mutant proteins such as α-synuclein,[80] huntingtin,[81] or tau mutant proteins[82] from the brains of transgenic mouse models. Our studies show that cytoplasmic aggregates and cell death can indeed be reduced upon treatment of RP11-RPE cells for 7 days with Rapamycin. However, other pharmacological treatments targeting autophagy (trehalose), ER stress (Salubrinal and STF-083010) or inducers of HSPs such as Arimoclomol had no beneficial effects in reducing the volume of cytoplasmic aggregates in RP11-RPE cells at the concentrations used. Our results are in agreement with other studies using Drosophila[83] and mouse models[84] associated with aggregate-prone proteins, showing the clearance of cytoplasmic aggregates after treatments in RP11-RPE cells with Rapamycin, demonstrating its potential therapeutic use in diseases associated with aggregate accumulation.[83,85] The improved aggregate clearance by activation of autophagy via Rapamycin administration indicates that it is the progressive aggregate accumulation that overburdens the waste disposal machinery rather than direct PRPF31 initiated misplicing. Hence, therapeutic strategies aiming at waste disposal activation present an important approach that needs to be investigated in close conjunction with gene therapy studies. The reduced wild-type PRPF31 protein expression together with the lack of inclusion of mutant PRPF31 in the active spliceosome corroborates the haploinsufficiency as pathomechanism and substantiates AAV.PRPF31 gene augmentation as an optimal approach for gene therapy treatment for RP11. Whilst this is useful in the early stages of the disease onset, where aggregate accumulation has not progressed, treatment at the later stages could combine the gene therapy with activation of autophagy. A recent paper has identified two FDA approved compounds, which reliably increase autophagic flux in RPE, while preserving RPE cell health and function.[86] Future studies should focus on testing these compounds with respect to prevent aggregate accumulation in PRPF31-RPE cells and the pharmacogenetic profile (e.g., crossing the blood–retina barrier, biodistribution, etc).

CONFLICT OF INTEREST

The authors declare that there is no conflict of interest that could be perceived as prejudicing the impartiality of the research reported.

ORCID

Majlinda Lako https://orcid.org/0000-0003-1327-8573

REFERENCES

1. Sweeney P, Park H, Baumann M, et al. Protein misfolding in neurodegenerative diseases: implications and strategies. *Transl Neurodegener*. 2017;6:6.
2. Soto C, Pritzkow S. Protein misfolding, aggregation, and conformational strains in neurodegenerative diseases. *Nat Neurosci*. 2018;21(10):1332-1340.
3. Surgucheva I, Ninkina N, Buchman VL, Grasing K, Surguchov A. Protein aggregation in retinal cells and approaches to cell protection. *Cell Mol Neurobiol*. 2005;25(6):1051-1066.

4. Hartong DT, Berson EL, Dryja TP. Retinitis pigmentosa. *Lancet*. 2006;368(9549):1795-1809.

5. McKie AB, McHale JC, Keen TJ, et al. Mutations in the pre-mRNA splicing factor gene PRPC8 in autosomal dominant retinitis pigmentosa (RP13). *Hum Mol Genet*. 2001;10(15):1555-1562.

6. Illing ME, Rajan RS, Bence NF, Kopito RR. A rhodopsin mutant linked to autosomal dominant retinitis pigmentosa is prone to aggregate and interacts with the ubiquitin proteasome system. *J Biol Chem*. 2002;277(37):34150-34160.

7. Saliba RS, Munro PM, Luthert PJ, Cheetham ME. The cellular fate of mutant rhodopsin: quality control, degradation and aggresome formation. *J Cell Sci*. 2002;115(Pt 14):2907-2918.

8. Vithana EN, Abu-Safieh L, Allen MJ, et al. A human homolog of yeast pre-mRNA splicing gene, PRP31, underlies autosomal dominant retinitis pigmentosa on chromosome 19q13.4 (RP11). *Mol Cell*. 2001;8(2):375-381.

9. Utz VM, Beight CD, Marino MJ, Hagstrom SA, Traboulsi EI. Autosomal dominant retinitis pigmentosa secondary to pre-mRNA splicing-factor gene PRPF31 (RP11): Review of disease mechanism and report of a family with a novel 3-base pair insertion. *Ophthalmic Genet*. 2013;34(4):183-188.

10. Buskin A, Zhu L, Chichagova V, et al. Disrupted alternative splicing for genes implicated in splicing and ciliogenesis causes PRPF31 retinitis pigmentosa. *Nat Commun*. 2018;9(1):4234.

11. Comitato A, Spampanato C, Chakarova C, Sanges D, Bhattacharya SS, Marigo V. Mutations in splicing factor PRPF3, causing retinal degeneration, form detrimental aggregates in photoreceptor cells. *Hum Mol Genet*. 2007;16(14):1699-1707.

12. Waseem NH, Vaclavik V, Webster A, Jenkins SA, Bird AC, Bhattacharya SS. Mutations in the gene coding for the pre-mRNA splicing factor, PRPF31, in patients with autosomal dominant retinitis pigmentosa. *Invest Ophthalmol Vis Sci*. 2007;48(3):1330-1334.

13. Valdés-Sánchez L, Calado SM, de la Cerda B, et al. Retinal pigment epithelium degeneration caused by aggregation of PRPF31 and the role of HSP70 family of proteins. *Mol Med*. 2019;26(1):1.

14. Hyttinen JM, Amadio M, Viiri J, Pascale A, Salminen A, Kaarniranta K. Clearance of misfolded and aggregated proteins by aggrephagy and implications for aggregation diseases. *Ageing Res Rev*. 2014;18:16-28.

15. Regent F, Morizur L, Lesueur L, et al. Automation of human pluripotent stem cell differentiation toward retinal pigment epithelial cells for large-scale productions. *Sci Rep*. 2019;9(1):10646.

16. Yildirim A, Mozaffari-Jovin S, Wallisch AK, et al. SANS (USH1G) regulates pre-mRNA splicing by mediating the intra-nuclear transfer of tri-snRNP complexes. *Nucleic Acids Res*. 2021;49(10):5845-5866.

17. Schaffert N, Hossbach M, Heintzmann R, Achsel T, Luhrmann R. RNAi knockdown of hPrp31 leads to an accumulation of U4/U6 di-snRNPs in Cajal bodies. *EMBO J*. 2004;23(15):3000-3009.

18. Cerniauskas E, Kurzawa-Akanbi M, Xie L, et al. Complement modulation reverses pathology in Y402H-retinal pigment epithelium cell model of age-related macular degeneration by restoring lysosomal function. *Stem Cells Transl Med*. 2020;9(12):1585-1603.

19. Abokyi S, Shan SW, To CH, Chan HH, Tse DY. Autophagy upregulation by the TFEB inducer trehalose protects against oxidative damage and cell death associated with NRF2 inhibition in human RPE cells. *Oxid Med Cell Longev*. 2020;2020:5296341.

20. Parfitt DA, Aguila M, McCulley CH, et al. The heat-shock response co-inducer arimoclomol protects against retinal degeneration in rhodopsin retinitis pigmentosa. *Cell Death Dis*. 2014;5:e1236.

21. Matsuoka M, Komoike Y. Experimental evidence shows salubrinal, an eIF2alpha dephosphorylation inhibitor, reduces xenotoxicant-induced cellular damage. *Int J Mol Sci*. 2015;16(7):16275-16287.

22. Barez SR, Atar AM, Aghaei M. Mechanism of inositol-requiring enzyme 1-alpha inhibition in endoplasmic reticulum stress and apoptosis in ovarian cancer cells. *J Cell Commun Signal*. 2020;14(4):403-415.

23. Zhou Y, Zhou B, Pache L, et al. Metascape provides a biologist-oriented resource for the analysis of systems-level datasets. *Nat Commun*. 2019;10(1):1523.

24. Tyanova S, Temu T, Sinitcyn P, et al. The Perseus computational platform for comprehensive analysis of (prote)omics data. *Nat Methods*. 2016;13(9):731-740.

25. Campbell M, Humphries M, Kennan A, Kenna P, Humphries P, Brankin B. Aberrant retinal tight junction and adherens junction protein expression in an animal model of autosomal dominant Retinitis pigmentosa: The Rho(-/-) mouse. *Exp Eye Res*. 2006;83(3):484-492.

26. Girard C, Will CL, Peng J, et al. Post-transcriptional spliceosomes are retained in nuclear speckles until splicing completion. *Nat Commun*. 2012;3:994.

27. Spector DL, Lamond AI. Nuclear speckles. *Cold Spring Harb Perspect Biol*. 2011;3(2):a000646.

28. Derlig K, Giessl A, Brandstatter JH, Enz R, Dahlhaus R. Special characteristics of the transcription and splicing machinery in photoreceptor cells of the mammalian retina. *Cell Tissue Res*. 2015;362(2):281-294.

29. Novotny I, Malinova A, Stejskalova E, et al. SART3-Dependent Accumulation of Incomplete Spliceosomal snRNPs in Cajal Bodies. *Cell Rep*. 2015;10(3):429-440.

30. Tyzack GE, Luisier R, Taha DM, et al. Widespread FUS mislocalization is a molecular hallmark of amyotrophic lateral sclerosis. *Brain*. 2019;142(9):2572-2580.

31. Butler JM, Supharattanasitthi W, Yang YC, Paraoan L. RNA-seq analysis of ageing human retinal pigment epithelium: Unexpected up-regulation of visual cycle gene transcription. *J Cell Molec Med*. 2021;25(12):5572-5585.

32. Maw MA, Kennedy B, Knight A, et al. Mutation of the gene encoding cellular retinaldehyde-binding protein in autosomal recessive retinitis pigmentosa. *Nat Genet*. 1997;17(2):198-200.

33. Eichers ER, Green JS, Stockton DW, et al. Newfoundland rod-cone dystrophy, an early-onset retinal dystrophy, is caused by splice-junction mutations in RLBP1. *Am J Human Genet*. 2002;70(4):955-964.

34. Kiser PD, Golczak M, Palczewski K. Chemistry of the retinoid (visual) cycle. *Chem Rev*. 2014;114(1):194-232.

35. Butler JM, Supharattanasitthi W, Yang YC, Paraoan L. RNA-seq analysis of ageing human retinal pigment epithelium: Unexpected up-regulation of visual cycle gene transcription. *J Cell Mol Med*. 2021;25(12):5572-5585.

36. Geuens T, Bouhy D, Timmerman V. The hnRNP family: Insights into their role in health and disease. *Hum Genet*. 2016;135(8):851-867.

37. Chen Q, Jin M, Zhu J, Xiao Q, Zhang L. Functions of heterogeneous nuclear ribonucleoproteins in stem cell potency and differentiation. *Biomed Res Int*. 2013;2013:623978.

38. Keppetipola NM, Yeom KH, Hernandez AL, Bui T, Sharma S, Black DL. Multiple determinants of splicing repression activity in the polypyrimidine tract binding proteins, PTBP1 and PTBP2. *RNA*. 2016;22(8):1172-1180.

39. Polydorides AD, Okano HJ, Yang YY, Stefani G, Darnell RB. A brain-enriched polypyrimidine tract-binding protein antagonizes the ability of Nova to regulate neuron-specific alternative splicing. *Proc Natl Acad Sci USA*. 2000;97(12):6350-6355.

40. Ao X, Zou L, Wu Y. Regulation of autophagy by the Rab GTPase network. *Cell Death Differ*. 2014;21(3):348-358.

41. Kohnke M, Delon C, Hastie ML, et al. Rab GTPase prenylation hierarchy and its potential role in choroideremia disease. *PLoS One*. 2013;8(12):e81758.

42. Eskelinen EL, Saftig P. Autophagy: A lysosomal degradation pathway with a central role in health and disease. *Biochim Biophys Acta*. 2009;1793(4):664-673.

43. Zhao YG, Zhang H. Autophagosome maturation: An epic journey from the ER to lysosomes. *J Cell Biol*. 2019;218(3):757-770.

44. Kinchen JM, Ravichandran KS. Phagosome maturation: going through the acid test. *Nat Rev Mol Cell Biol*. 2008;9(10):781-795.

45. Malinova A, Cvackova Z, Mateju D, et al. Assembly of the U5 snRNP component PRPF8 is controlled by the HSP90/R2TP chaperones. *J Cell Biol*. 2017;216(6):1579-1596.

46. Wolf DH, Hilt W. The proteasome: A proteolytic nanomachine of cell regulation and waste disposal. *Biochim Biophys Acta*. 2004;1695(1-3):19-31.

47. Komander D, Rape M. The ubiquitin code. *Annu Rev Biochem*. 2012;81:203-229.

48. Tanaka K. The proteasome: Overview of structure and functions. *Proc Jpn Acad Ser B Phys Biol Sci*. 2009;85(1):12-36.

49. Lilienbaum A. Relationship between the proteasomal system and autophagy. *Int J Biochem Mol Biol*. 2013;4(1):1-26.

50. Klionsky DJ, Abdel-Aziz AK, Abdelfatah S, et al. Guidelines for the use and interpretation of assays for monitoring autophagy. *Autophagy*. 2021;17(1):1-382.

51. Ciechanover A, Kwon YT. Degradation of misfolded proteins in neurodegenerative diseases: Therapeutic targets and strategies. *Exp Mol Med*. 2015;47:e147.

52. Takalo M, Salminen A, Soininen H, Hiltunen M, Haapasalo A. Protein aggregation and degradation mechanisms in neurodegenerative diseases. *Am J Neurodegener Dis*. 2013;2(1):1-14.

53. Luo M, Lu Z, Sun H, et al. Nuclear entry of active caspase-3 is facilitated by its p3-recognition-based specific cleavage activity. *Cell Res*. 2010;20(2):211-222.

54. Benatar M, Wuu J, Andersen PM, et al. Randomized, double-blind, placebo-controlled trial of arimoclomol in rapidly progressive. *Neurology*. 2018;90(7):e565-e74.

55. Vígh L, Literáti PN, Horváth I, et al. Bimoclomol: A nontoxic, hydroxylamine derivative with stress protein-inducing activity and cytoprotective effects. *Nat Med*. 1997;3(10):1150-1154.

56. Kieran D, Kalmar B, Dick JR, Riddoch-Contreras J, Burnstock G, Greensmith L. Treatment with arimoclomol, a coinducer of heat shock proteins, delays disease progression in ALS mice. *Nat Med*. 2004;10(4):402-405.

57. Liu L, Xu L, Zhang S, et al. STF-083010, an inhibitor of XBP1 splicing, attenuates acute renal failure in rats by suppressing endoplasmic reticulum stress-induced apoptosis and inflammation. *Exp Anim*. 2018;67(3):373-382.

58. Huang X, Chen Y, Zhang H, Ma Q, Zhang YW, Xu H. Salubrinal attenuates β-amyloid-induced neuronal death and microglial activation by inhibition of the NF-κB pathway. *Neurobiol Aging*. 2012;33(5):1007.e9-17.

59. Saxena S, Cabuy E, Caroni P. A role for motoneuron subtype-selective ER stress in disease manifestations of FALS mice. *Nat Neurosci*. 2009;12(5):627-636.

60. Wang ZF, Gao C, Chen W, et al. Salubrinal offers neuro-protection through suppressing endoplasmic reticulum stress, autophagy and apoptosis in a mouse traumatic brain injury model. *Neurobiol Learn Mem*. 2019;161:12-25.

61. Zhang J, Bai Y, Huang L, et al. Protective effect of autophagy on human retinal pigment epithelial cells against lipofuscin fluorophore A2E: Implications for age-related macular degeneration. *Cell Death Dis*. 2015;6:e1972.

62. Feldman ME, Apsel B, Uotila A, et al. Active-site inhibitors of mTOR target rapamycin-resistant outputs of mTORC1 and mTORC2. *PLoS Biol*. 2009;7(2):e38.

63. Thellung S, Corsaro A, Nizzari M, Barbieri F, Florio T. Autophagy activator drugs: A new opportunity in neuroprotection from misfolded protein toxicity. *Int J Mol Sci*. 2019;20(4):901.

64. Bushehri A, Zare-Abdollahi D, Alavi A, Dehghani A, Mousavimikala M, Khorram Khorshid HR. Identification of PROS1 as a novel candidate gene for juvenile retinitis pigmentosa. *Int J Mol Cell Med*. 2019;8(3):179-190.

65. Sultan N, Ali I, Bukhari SA, et al. A novel mutation in RDH5 gene causes retinitis pigmentosa in consanguineous Pakistani family. *Genes Genomics*. 2018;40(5):553-559.

66. Waterham HR, Ferdinandusse S, Wanders RJA. Human disorders of peroxisome metabolism and biogenesis. *Bba-Mol Cell Res*. 2016;1863(5):922-933.

67. Zhang L, Sun Z, Zhao P, et al. Whole-exome sequencing revealed HKDC1 as a candidate gene associated with autosomal-recessive retinitis pigmentosa. *Hum Mol Genet*. 2018;27(23):4157-4168.

68. Xue Y, Shen SQ, Jui J, et al. CRALBP supports the mammalian retinal visual cycle and cone vision. *J Clin Invest*. 2015;125(2):727-738.

69. Hipp S, Zobor G, Glockle N, et al. Phenotype variations of retinal dystrophies caused by mutations in the RLBP1 gene. *Acta Ophthalmol*. 2015;93(4):e281-6.

70. Reddy VS, Raghu G, Reddy SS, Pasupulati AK, Suryanarayana P, Reddy GB. Response of small heat shock proteins in diabetic rat retina. *Invest Ophthalmol Vis Sci*. 2013;54(12):7674-7682.

71. Tai HC, Serrano-Pozo A, Hashimoto T, Frosch MP, Spires-Jones TL, Hyman BT. The synaptic accumulation of hyperphosphorylated tau oligomers in Alzheimer disease is associated with dysfunction of the ubiquitin-proteasome system. *Am J Pathol*. 2012;181(4):1426-1435.

72. Andre R, Tabrizi SJ. Misfolded PrP and a novel mechanism of proteasome inhibition. *Prion*. 2012;6(1):32-36.

73. Lindersson E, Beedholm R, Hojrup P, et al. Proteasomal inhibition by alpha-synuclein filaments and oligomers. *J Biol Chem*. 2004;279(13):12924-12934.

74. Gregori L, Fuchs C, Figueiredo-Pereira ME, Van Nostrand WE, Goldgaber D. Amyloid beta-protein inhibits

ubiquitin-dependent protein degradation in vitro. *J Biol Chem*. 1995;270(34):19702-19708.

75. Qi L, Zhang XD, Wu JC, et al. The role of chaperone-mediated autophagy in huntingtin degradation. *PLoS One*. 2012;7(10):e46834.

76. Martinez-Vicente M, Talloczy Z, Wong E, et al. Cargo recognition failure is responsible for inefficient autophagy in Huntington's disease. *Nat Neurosci*. 2010;13(5):567-576.

77. Intartaglia D, Giamundo G, Conte I. Autophagy in the retinal pigment epithelium: a new vision and future challenges. *Febs Journal*. 2021.

78. Louneva N, Cohen JW, Han LY, et al. Caspase-3 is enriched in postsynaptic densities and increased in Alzheimer's disease. *Am J Pathol*. 2008;173(5):1488-1495.

79. Falasconi A, Biagioni M, Novelli E, Piano I, Gargini C, Strettoi E. Retinal phenotype in the rd9 mutant mouse, a model of X-Linked RP. *Front Neurosci*. 2019;13:991.

80. Webb JL, Ravikumar B, Atkins J, Skepper JN, Rubinsztein DC. Alpha-Synuclein is degraded by both autophagy and the proteasome. *J Biol Chem*. 2003;278(27):25009-25013.

81. Sarkar S, Rubinsztein DC. Huntington's disease: Degradation of mutant huntingtin by autophagy. *FEBS J*. 2008;275(17):4263-4270.

82. Rodriguez-Navarro JA, Cuervo AM. Autophagy and lipids: Tightening the knot. *Semin Immunopathol*. 2010;32(4):343-353.

83. Berger Z, Ravikumar B, Menzies FM, et al. Rapamycin alleviates toxicity of different aggregate-prone proteins. *Hum Mol Genet*. 2006;15(3):433-442.

84. Ravikumar B, Vacher C, Berger Z, et al. Inhibition of mTOR induces autophagy and reduces toxicity of polyglutamine expansions in fly and mouse models of Huntington disease. *Nat Genet*. 2004;36(6):585-595.

85. Ravikumar B, Duden R, Rubinsztein DC. Aggregate-prone proteins with polyglutamine and polyalanine expansions are degraded by autophagy. *Hum Mol Genet*. 2002;11(9):1107-1117.

86. Zhang QT, Presswalla F, Ali RR, Zacks DN, Thompson DA, Miller JML. Pharmacologic activation of autophagy without direct mTOR inhibition as a therapeutic strategy for treating dry macular degeneration. *Aging-Us*. 2021;13(8):10866-10890.

SUPPORTING INFORMATION

Additional supporting information may be found in the online version of the article at the publisher's website.